scientific reports

Check for updates

OPEN

DFT investigation of CO_2 activation and carbon trapping at Ni/Al_2O_3 interfaces in dry reforming of methane

Salah Sakrane[1], Oualid Alioui[1], Leila Dehimi[1,2], Marco Balsamo[3], Alessandro Erto[4], Mohammed Alamro[5], Malik Albrahim[5], K. S. Abdel Halim[5], Byong-Hun Jeon[6]✉, Hyun-Jo Ahn[6] & Yacine Benguerba[1]✉

Dry reforming of methane over Ni catalysts offers a route to convert CH_4 and CO_2 into syngas while using two greenhouse gases, but its performance is limited by carbon deposition and poorly understood metal support effects. Here, density functional theory with DFT + U+D2 is used to study a Ni dimer (Ni2) supported on α Al_2O_3(0001) and hydroxylated α Al_2O_3 OH(0001). After validating the structural model against reference data, we examine adsorption of CH_4, CO_2, CO, H_2, and atomic C on bare and Ni-supported surfaces. CH_4 and H_2 show weak, nearly system-independent physisorption, indicating that their activation must occur mainly in the transition states. In contrast, CO_2 and CO are strongly chemisorbed and activated at Ni Al_2O_3 interfaces, especially on the hydroxylated surface, where large adsorption energies, strong bending, and marked charge transfer are found. Atomic carbon is very strongly stabilized at the same interfacial sites. Analysis of projected density of states, Mulliken charges and electron density differences identifies the Ni alumina perimeter as the key region governing CO_2 activation and coke formation in Ni-based DRM catalysts.

Keywords Dry reforming of methane (DRM), Density functional theory (DFT), Ni-based catalyst (NBC), Carbon dioxide activation, Alumina support

Carbon dioxide (CO_2) is widely recognized as a major greenhouse gas (GHG) contributing to global warming and driving significant climate change[1]. Consequently, extensive research over recent decades has focused on developing viable industrial strategies to mitigate its environmental impact. Among the different approaches proposed, the catalytic conversion of CO_2 into valuable chemicals and fuels has emerged as a promising pathway for reducing greenhouse gas emissions. Several thermochemical processes, such as CO_2 hydrogenation[2], methanation[3], the reverse water-gas shift reaction[4], and the dry reforming of methane (DRM)[5], have been explored for this purpose. Among them, DRM has attracted particular interest due to its dual environmental and industrial benefits[6].

The DRM process simultaneously consumes CO_2 and CH_4, converting them into syngas with an H_2/CO ratio close to unity, a composition ideally suited for downstream applications such as Fischer–Tropsch synthesis and the production of oxygenated chemicals[7,8]. However, DRM is a highly endothermic reaction, as described by Eq. (1), typically requiring temperatures between 700 and 850 °C to achieve effective conversion. These harsh operating conditions necessitate the use of efficient and stable catalysts capable of sustaining high activity and selectivity[9].

$$\boldsymbol{CH_4 + CO_2 \leftrightarrow 2CO + 2H_2}, \qquad \boldsymbol{\Delta H^{\circ}_{298K} = +247\ kJ/mol} \tag{1}$$

[1]Laboratoire de Biopharmacie Et Pharmacotechnie (LBPT), Faculty of Technology, Université Sétif 1, Ferhat ABBAS, Setif, Algeria. [2]Faculté des Sciences, Université Ferhat Abbas Setif 1, Setif, Algeria. [3]Dipartimento di Scienze Chimiche, Università degli Studi di Napoli Federico II, Complesso Universitario di Monte Sant'Angelo, Napoli 80126, Italy. [4]Dipartimento di Ingegneria Chimica, dei Materiali e della Produzione Industriale, Università di Napoli Federico II, P. leTecchio, 80, Napoli 80125, Italy. [5]Chemical Engineering Department, College of Engineering, University of Ha'il, P.O. Box 2440, Ha'il 81441, Saudi Arabia. [6]Department of Earth Resources and Environmental Engineering, Hanyang University, 222 Wangsimni- ro, Seongdong-gu, Seoul 04763, Republic of Korea. ✉email: bhjeon@hanyang.ac.kr; benguerbayacine@yahoo.fr

Catalyst deactivation remains a major challenge in DRM, primarily due to metal sintering and carbon deposition on the catalyst surface[10]. This has driven extensive research into developing highly active and coking-resistant systems. Although noble metal catalysts such as Rh, Ru, Pt, and Pd exhibit excellent performance and resistance to carbon formation[11,12], their high cost limits their large-scale industrial deployment. Transition metals, including Ni, Co, Cu, and Fe, offer a more cost-effective alternative and have demonstrated competitive activity[13]. Among them, Ni-based catalysts are the most widely studied due to their high performance, abundance, and affordability[14,15]. Nevertheless, Ni catalysts remain susceptible to deactivation through carbon deposition and nanoparticle sintering, leading to the progressive loss of active sites[16].

The magnitude of the underlying environmental challenge is substantial. According to the International Energy Agency (IEA), global methane emissions reached approximately 356 million tonnes in 2022, highlighting the industrial significance of DRM as a promising route for methane valorisation and greenhouse gas mitigation[17]. Under industrially relevant conditions, conventional Ni/Al_2O_3 catalysts exhibit CH_4 conversions ranging from 36% to 59% at 700 °C, with their performance being highly dependent on both Ni loading and operating temperature[18].

More recently, hydroxyl-engineered Ni/Al_2O_3 catalysts have delivered CH_4 and CO_2 conversions of 88% and 90%, respectively, while exhibiting stable catalytic performance over 50 h of continuous operation[19]. These findings underscore both the industrial potential of Ni/Al_2O_3 catalysts and the persistent discrepancy between laboratory-scale performance and the long-term operational stability required for commercial implementation, which is largely governed by carbon-induced deactivation at the metal–support interface. Carbon formation in DRM mainly arises from the Boudouard reaction (Eq. 2) and methane cracking (Eq. 3):

$$2CO \leftrightarrow \ C + CO_2, \quad \Delta H^{\circ}_{298K} = -173\ kJ/mol \tag{2}$$

$$CH_4 \leftrightarrow \ C + 2H_2, \quad \Delta H^{\circ}_{298K} = +74.84\ kJ/mol \tag{3}$$

A key strategy to mitigate these issues involves tailoring metal oxide supports, which significantly influence catalyst performance through modifications in metal–support interactions, dispersion, and particle size[20]. The physicochemical properties of supports—such as reducibility, basicity, and oxygen storage capacity—play a crucial role in determining catalytic behaviour. Consequently, various oxides, including Al_2O_3, ZrO_2, SiO_2, TiO_2, and CeO_2, have been extensively investigated as supports for DRM catalysts[21]. Among these, Al_2O_3 remains one of the most commonly employed supports due to its mechanical robustness, thermal stability, abundance, and low cost[22,23].

Promoters have also been widely employed to enhance catalytic performance and suppress coke formation. For instance, noble metals or alkaline promoters can significantly improve catalyst stability[24]. A. H. Fakeeha et al.[25] demonstrated that Fe-promoted Ni catalysts supported on ZrO_2–Al_2O_3 displayed enhanced DRM activity, with the 5Ni + 3Fe–10Zr + Al formulation achieving CH_4 and CO_2 conversions of 87% and 90%, respectively, alongside an H_2/CO ratio of 0.98. Similarly, A. M. Manabayeva et al.[26] reported superior stability in Ni–Mn–Al trimetallic catalysts, with the 15Ni–15Mn–20Al system sustaining syngas production at 850 °C for 20 h. In contrast, Al-free catalysts exhibited greater acidity, increased coking, and diminished activity. D. G. Araiza et al.[27] further showed that Pt–Ni/CeO_2 bimetallic catalysts outperform their monometallic counterparts due to improved metal dispersion, ceria reducibility, and coke resistance, with the 50:50 Pt: Ni system exhibiting the most balanced performance. In another study, Alipour et al.[28] assessed alkaline earth promoters on Ni/Al_2O_3 catalysts and reported that MgO improved CH_4 conversion and suppressed carbon deposition, whereas CaO and BaO led to diminished activity.

Recent advances have expanded beyond classical supported Ni nanoparticles, with growing interest in sub-nanometric metal species and dimer-supported catalysts. Previous studies demonstrated that supported Pd_2 species exhibit excellent CO_2 activation in water-gas shift reactions[29], while Mn dimers improve O_2 dissociation and NO_x oxidation due to their unique electronic structures[30]. Ni_2 clusters have also been identified as highly reactive species for O_2 activation on YSZ(111)[31]. Moreover, the stability of Ni dimers on α-Al_2O_3(0001) surfaces has been explored, although the influence of surface hydroxylation and the interaction of Ni_2 with DRM reactants remain insufficiently understood[32]. Given that metal–support interactions largely determine catalytic behaviour, a detailed understanding of the electronic structure of Ni dimers on alumina is essential.

Quantum chemical approaches such as Density Functional Theory (DFT) provide invaluable insight into the atomic and electronic structure of catalysts, enabling the investigation of adsorption phenomena and reaction intermediates at the molecular scale[33]. In particular, recent DFT studies have provided a detailed view of how the size and composition of Ni-based active phases govern CO_2 activation and the formation of CO during DRM. Niu et al. used DFT to show that the Ni particle size on a MgO support markedly modifies the preferred pathway for CO_2 activation, with very small Nix clusters favouring direct CO_2 dissociation while larger ones favour a hydrogenation-assisted route, and they correlated these trends with the resistance of the catalyst to carbon deposition[34]. Zhang et al. further explored how alloying Ni with Cu reshapes the CO formation pathways during DRM by modifying the electronic structure of the Ni surface and the relative stability of CHxO intermediates, highlighting how second-metal doping can be used to steer the selectivity and coke tolerance of Ni-based catalysts[35]. These works underscore the role of DFT, and in particular DFT + U calculations on supported Ni systems, as an indispensable tool for unraveling the molecular-level descriptors of activity and coke resistance, and they motivate the use of similar tools to investigate the present Ni dimer/α-Al_2O_3 systems.

In this study, DFT calculations are employed to investigate the adsorption behaviour of key DRM species on both hydroxylated and non-hydroxylated α-Al_2O_3(0001) surfaces. By examining stable adsorption modes, metal–support interactions, and the electronic characteristics of supported Ni dimer using DOS, PDOS, EDD,

and Mulliken charge analysis, this work provides a deeper understanding of the catalytic properties and stability of Ni_2/Al_2O_3 systems in DRM environments.

Computational Details

All first-principles calculations were performed using the CASTEP module implemented in Materials Studio[36], which employs a plane-wave basis set within the framework of Kohn–Sham Density Functional Theory (DFT). Exchange–correlation interactions were described using the Perdew–Burke–Ernzerhof (PBE) functional[37] formulated within the Generalized Gradient Approximation (GGA)[38]. Long-range dispersion forces, which are known to influence adsorption energies and the stability of weakly bound intermediates, were incorporated via the Grimme DFT-D2 correction scheme. Spin polarization was explicitly applied to both isolated and surface-supported Ni dimer owing to the open-shell 3 d character of nickel.

To properly account for the strong electronic correlation associated with Ni 3 d electrons, the DFT + U method was incorporated using the rotationally invariant formalism of Dudarev et al., with an effective Hubbard parameter U_{eff} = 4.0 eV applied to the Ni 3 d orbitals. This value has been widely adopted for Ni-based catalytic systems and was shown to provide a good compromise between an accurate description of the localized Ni 3 d states and the correct prediction of magnetic and adsorption properties, in agreement with previous DFT + U studies on Ni clusters and supported Ni catalysts[34,35,39]. This correction improves the localization of Ni d states and enhances the accuracy of adsorption energies and metal–support interactions where standard GGA functionals typically underestimate electron correlation contributions.

Surface and Slab Construction

The α-Al_2O_3(0001) slab model was derived from the corundum bulk structure[40], using a hexagonal unit cell containing six Al_2O_3 formula units. Experimental lattice parameters (a = b = 4.759 Å, c = 12.991 Å) were adopted to ensure structural fidelity (Fig. 1).

The bulk crystal was cleaved along the (0001) plane to construct a 2 × 2 surface supercell with dimensions of 9.52 × 9.52 × 18.84 $Å^3$. The slab comprises two Al layers and four O layers (40 atoms total). This slab thickness was selected as the minimum required to converge the surface energy of α-Al_2O_3(0001) and to recover bulk-like Al–O coordination at the central layers, in line with several previous theoretical studies of the same surface[41–43], while keeping the system computationally tractable when combined with the Ni dimer and the various adsorbates. The chosen 2 × 2 lateral expansion further ensures that the lateral spacing between periodic images of the adsorbed Ni dimer and DRM molecules is large enough to avoid spurious adsorbate–adsorbate interactions, corresponding to a low-coverage regime suitable for studying intrinsic adsorption properties at the metal–support interface[44]. During structural optimizations, the topmost layers were allowed to relax while the bottom layers remained fixed to emulate bulk-like behavior. A vacuum space of 13 Å was introduced along the c-axis to eliminate interactions between periodic images and ensure accurate surface energetics.

To investigate metal–support interactions, the optimized Ni_2 dimer was placed at various adsorption sites on both pristine and hydroxylated α-Al_2O_3(0001) surfaces. Hydroxylated surfaces were generated based on experimentally and computationally observed OH coverages reported for alumina under relevant temperature and humidity conditions[36,45–50].

Computational Parameters

Geometry optimizations were carried out until the following convergence criteria were satisfied, maximum force < 0.05 eV·$Å^{-1}$, maximum stress < 0.1 GPa, maximum atomic displacement < 0.002 Å, and self consistent field [SCF] energy change < 2×10^{-6} eV per atom. A plane wave cutoff energy of 400 eV was adopted, which

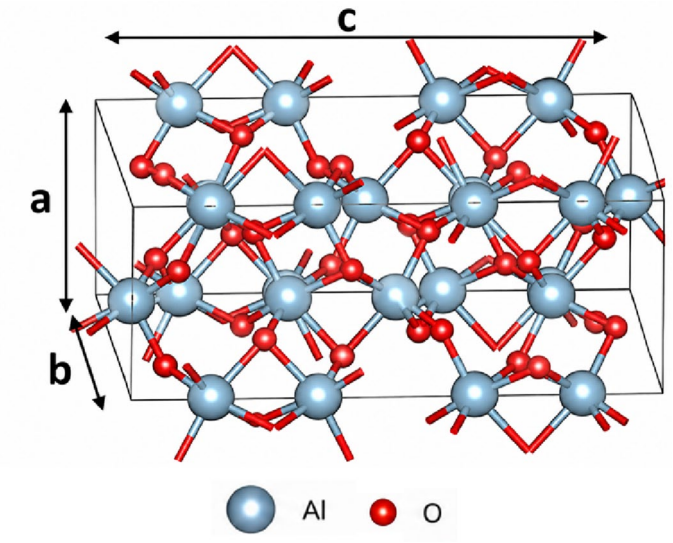


Fig. 1. Bulk structure of α-Al_2O_3.

provides a good compromise between accuracy and computational cost for the systems considered. Brillouin zone sampling was performed with a 2×2×12 Monkhorst Pack k point mesh, which was verified to yield converged total energies for the chosen cells. Ultrasoft on the fly generated [OTFG] pseudopotentials were used in order to reduce the plane wave basis size while preserving an accurate description of core valence electron interactions. The optimized bulk α Al_2O_3 structure yielded a cohesive energy of 2.105 eV per atom, in good agreement with literature data, confirming the reliability of the structural model.

Electronic Structure and Charge Analyses

Electronic structure calculations—including total Density of States (DOS), Projected DOS (PDOS), and Electron Density Difference (EDD) maps—were conducted to characterize bonding interactions between Ni dimer, the alumina surface, and adsorbates. EDD maps were generated using:

$$\Delta\rho = \rho_{Ni_2/surface} - \rho_{surface} - \rho_{Ni_2} \tag{4}$$

To visualize electron redistribution associated with adsorption or metal–support interactions. Mulliken population analysis was performed to assess partial charge transfer. Although Mulliken charges are basis-dependent, they remain useful for intra-study comparisons of electronic trends.

The Ni dimer binding energy was computed using:

$$E_{bind(2)} = \frac{\left[E_{(2)} - 2 \times E_{(\blacksquare)}\right]}{2} \tag{5}$$

where $E_{(2)}$ is the total energy of the optimized Ni_2 dimer, and $E_{(\blacksquare)}$ is the energy of a single isolated Ni atom.

Adsorption Energy Calculations

Adsorption energies of CH_4, CO_2, CO, H_2, and carbon species on the isolated Ni_2 dimer and supported Ni_2/α-Al_2O_3(0001) models were calculated as:

$$E_{ads} = E_{\frac{adsorbates}{slab}} - E_{slab} - E_{adsorbates} \tag{6}$$

where:

- $E_{\frac{adsorbates}{slab}}$ is the total energy of the adsorbate–surface system,
- E_{slab} is the energy of the clean support (with or without Ni_2), and.
- $E_{adsorbates}$ is the energy of the isolated molecule.

Negative E_{ads} values denote exothermic, thermodynamically favorable adsorption.

Results and discussion

Structural relaxations

Table 1 summarizes the calculated bond lengths for the optimized gas-phase reference species employed in this study. The values are in very good agreement with recent experimental and theoretical data, which supports the reliability of the computational protocol used here[31,51–57]. This consistency with the literature indicates that the chosen DFT level is suitable for accurately describing both small molecules and metallic species relevant to the Ni/α-Al_2O_3 systems.

For CH_4, the computed C-H bond length of 1.09 Å reproduces exactly the reported values. Similarly, the calculated H-H distance in H_2 (0.75 Å) is very close to both theoretical predictions and the experimental value of 0.74 Å, which confirms the robustness of the method for homonuclear diatomic molecules. The C-O bond lengths obtained for CO and CO_2 also match well with the literature, with deviations within 0.01 Å. Such small differences are typical of DFT calculations and fall within the expected accuracy of the method for covalent bonds.

The Ni-Ni bond distance in the Ni_2 dimer was computed as 2.38 Å, slightly larger than the theoretical value of 2.33 Å and moderately higher than the experimental value of 2.20 Å. This modest overestimation can be attributed to the known limitations of gas-phase DFT calculations for small metallic clusters, which are particularly sensitive to the choice of exchange correlation functional and spin state. Overall, the comparison in Table 1 confirms that the present DFT setup provides a quantitatively reliable description of both molecular

Gas	Bond length(Å)				
	This work	Theoretical	Ref.	Experimental	Ref.
CH_4	1.09	1.09	[51]	1.09	52
CO_2	1.17	1.16	[53]	1.16	54
CO	1.15	1.14	[55]	1.14	56
H_2	0.75	0.75	[57]	0.74	58
Ni_2	2.38	2.33	[31]	2.20	59

Table 1. Interatomic distances of the optimized structures.

and metallic bonding, and that the remaining discrepancies are within the usual uncertainty associated with differences in computational settings and experimental conditions.

Figure 2 displays the optimized geometries of the isolated Ni dimer and the α-Al_2O_3(0001) and α-Al_2O_3-OH(0001) surfaces. The corresponding binding energy, −1.17 eV, is close to the expected value of −1.02 eV[60], which further supports the suitability of the computational approach for describing the Ni dimer. Low-energy electron diffraction (LEED) measurements by Toofan et al.[61] showed that, after relaxation, the surface O and Al atoms of α-Al_2O_3(0001) and α-Al_2O_3-OH(0001) are nearly coplanar, a feature that is well reproduced by the present surface models.

Ni dimer supported structures on α-Al_2O_3(0001) and α-Al_2O_3-OH(0001) were obtained by systematically exploring different adsorption sites and orientations, including both perpendicular and parallel configurations of the dimer with respect to the surface. Only the most thermodynamically stable configurations are depicted in Fig. 3.

For the Ni dimer on the α-Al_2O_3(0001) surface, the most stable adsorption energy is −1.60 eV, which indicates a strong metal support interaction between metallic Ni and the alumina surface. In this configuration, each Ni atom is bonded to two surface O atoms: Ni1 to O3c-1 and O3c-2, and Ni2 to O3c-8 and O3c-21. Adsorption of Ni_2 induces local distortions in the alumina lattice. The Al3c-11–O3c-2, Al3c-11–O3c-21, Al3c-3–O3c-1, and Al3c-6–O3c-8 bond lengths increase from 1.70, 1.70, 1.70, and 1.91 Å to 1.78, 1.77, 1.75, and 1.80 Å, respectively. These elongations reflect the redistribution of electron density and the reorganization of the local coordination environment upon Ni adsorption.

For the Ni dimer adsorbed on the hydroxylated α-Al_2O_3-OH(0001) surface, the most stable adsorption energy is −1.85 eV, which is more exothermic than on the non-hydroxylated α-Al_2O_3(0001) surface. This stronger binding is attributed to the presence of surface hydroxyl groups, which enhance the thermodynamic stability of the Ni/support interface. In the most stable configuration, Ni1 is bonded to Al3c-3, Al3c-11, and O2c-25, while Ni2 interacts with Al3c-3, O3c-8, and O3c-21. As on the bare alumina surface, Ni adsorption induces structural relaxation of the hydroxylated support. The Al3c-11–O3c-2, Al3c-11–O3c-21, Al3c-3–O3c-1, and Al3c-6–O3c-8 bond lengths increase from 1.71, 1.71, 1.71, and 1.91 Å to 1.75, 1.77, 1.79, and 1.93 Å, respectively. The Ni1–Ni2 distance also increases from 2.39 to 2.41 Å, which suggests a slightly stronger perturbation of the Ni dimer geometry on the hydroxylated surface, in line with the larger adsorption energy.

The electronic consequences of Ni adsorption were examined through total density of states (DOS) calculations, as shown in Fig. 4. For both α-Al_2O_3(0001) and α-Al_2O_3-OH(0001), the DOS of the Ni-supported systems is shifted to lower energies compared with the bare supports, and the region near the Fermi level is strongly modified. In particular, the band gap (E_g) decreases from 3.30 eV to 1.02 eV for α-Al_2O_3(0001) and from 3.28 eV to 1.26 eV for α-Al_2O_3-OH(0001) upon Ni dimer adsorption. This significant narrowing of the band gap reflects the strong chemical interaction between the metallic Ni dimer and the alumina surfaces and indicates an increased electronic conductivity of the supported systems, which is relevant for catalytic applications. Specifically, projected density of states (PDOS) analyses (Supplementary Information, Figure S1) reveal that the new states populating the original alumina band gap are dominated by Ni 3d-derived contributions, with smaller but non-negligible mixing with the O 2p orbitals of surface oxygen atoms in the immediate vicinity of the Ni dimer and, on the hydroxylated surface, with the O 2p states of the OH groups. The newly formed Ni 3 d states lie in the region between the top of the alumina valence band (mainly O 2p in character) and the bottom of its conduction band (predominantly Al 3sp in character), bridging these two manifolds through hybridization. This Ni 3d–O 2p hybridization at the interface explains both the narrowing of the band gap and the appearance of states near the Fermi level that act as electron donors/acceptors for incoming adsorbates such as CO_2, CO and atomic C, in line with the Mulliken and EDD analyses presented in the next sections.

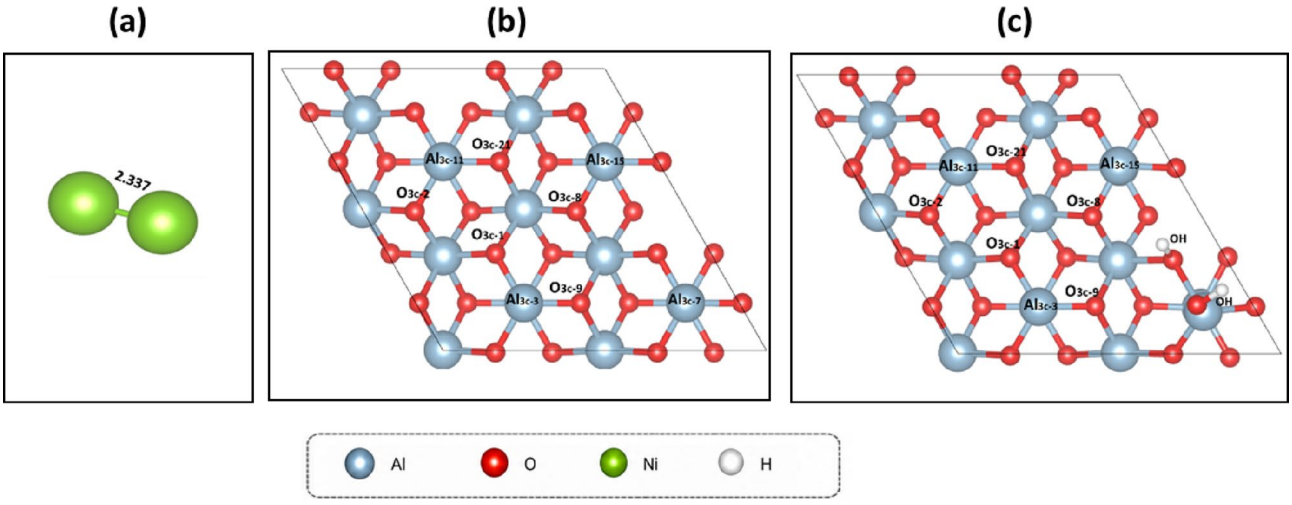


Fig. 2. The optimized structures of (**a**) isolated Ni dimer, (**b**) α-Al_2O_3(0001), and (**c**) α-Al_2O_3-OH (0001) surfaces.

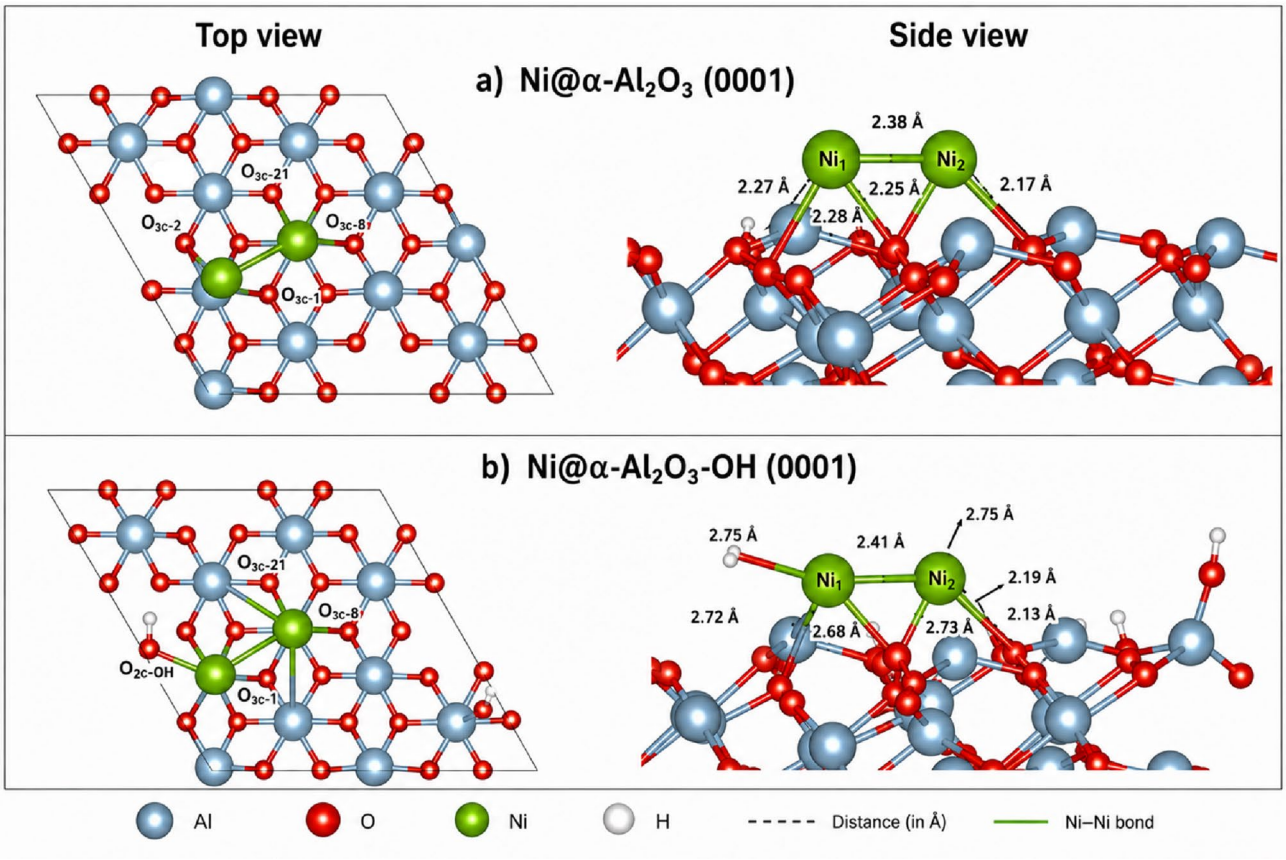


Fig. 3. Optimized structures of alumina-supported Ni dimer model catalysts obtained with the DFT + U+D2 scheme.

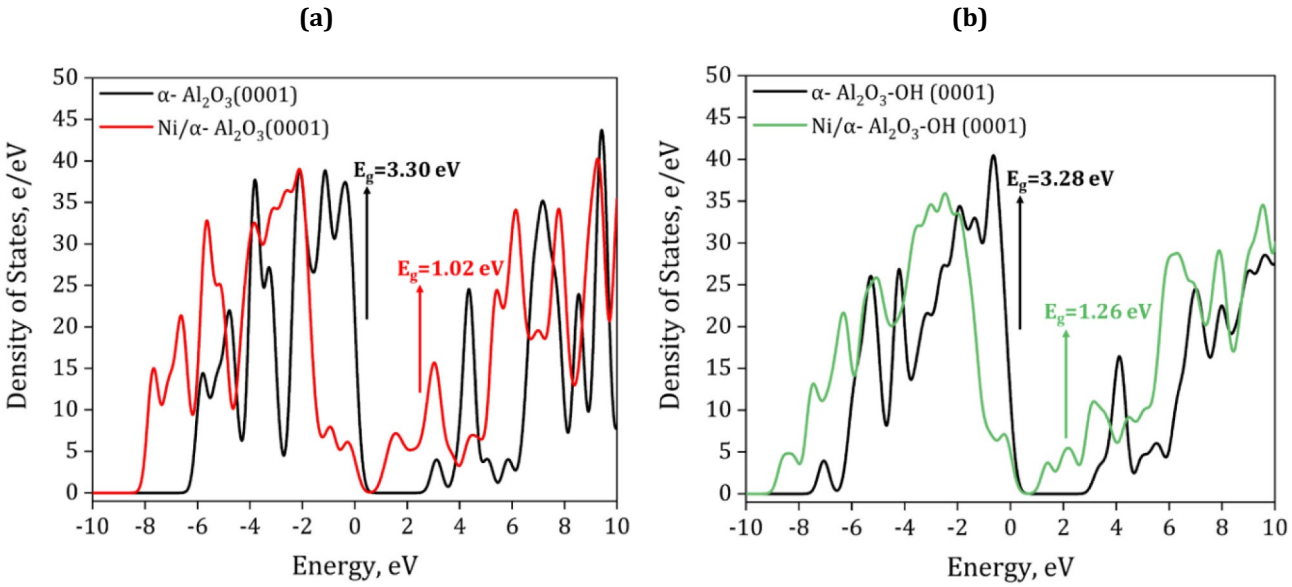


Fig. 4. Total DOS for (**a**) α-Al_2O_3(0001) and Ni/α-Al_2O_3(0001) systems, and (**b**) α-Al_2O_3-OH(0001) and Ni/α-Al_2O_3-OH(0001) systems.

	α-Al_2O_3(0001)	Ni/α-Al_2O_3(0001)	α-Al_2O_3-OH (0001)	Ni/α-Al_2O_3-OH (0001)
Ni_2	-	0.36	-	0.52
Oxygen				
O_{3c1}	−1.14	−1.09	-	-
O_{3c2}	−1.14	−1.08	-	-
O_{3c8}	−1.14	−1.06	−1.13	−1.06
O_{3c21}	−1.14	−1.09	−1.14	−1.08
O_{3c25}	-	-	−0.13	−1.04
Aluminum				
Al_{3c3}	-	-	1.79	1.29
Al_{3c11}	1.78	1.41	1.79	1.46

Table 2. Mulliken charges (e) of α-Al_2O_3 surfaces and Ni-supported systems.

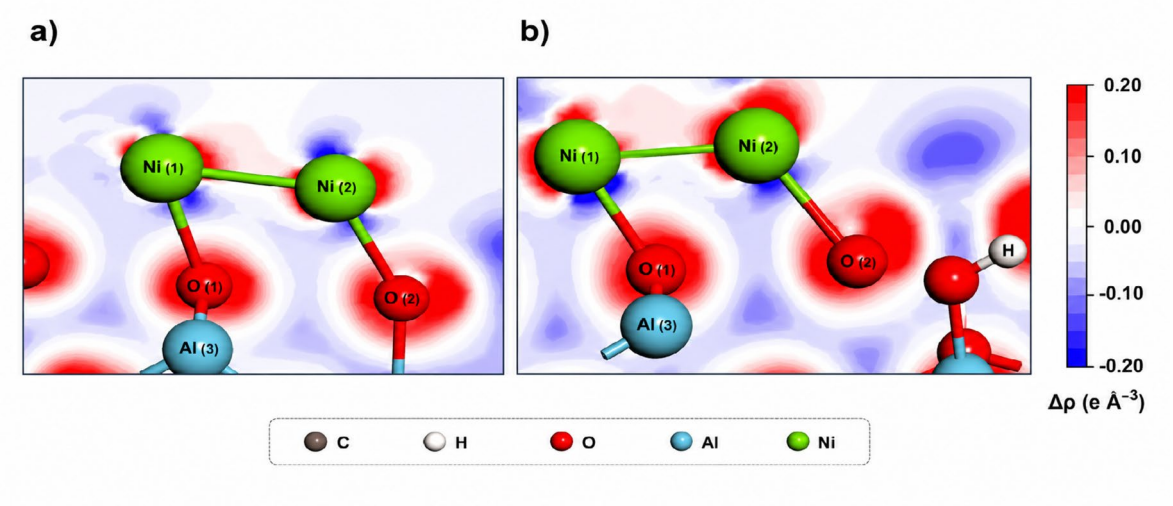


Fig. 5. EDD maps for Ni adsorption on (**a**) pure α-Al_2O_3(0001) and (**b**) hydroxylated α-Al_2O_3-OH(0001) surfaces.

To gain deeper insight into the nature of the metal support interaction, Mulliken charge (MC) analysis and electron density difference (EDD) mapping were performed. The Mulliken charges for α-Al_2O_3(0001), α-Al_2O_3-OH(0001), Ni/α-Al_2O_3(0001) and Ni/α-Al_2O_3-OH(0001) are collected in Table 2.

Deposition of the Ni dimer leads to net positive charges of + 0.36 e and + 0.52 e on the Ni atoms for the pure and hydroxylated α-Al_2O_3(0001) surfaces, respectively, which indicates electron transfer from Ni to the support. The larger positive charge on Ni in the hydroxylated system is consistent with the more negative adsorption energy and therefore points to a stronger metal support interaction on α-Al_2O_3-OH(0001). Concomitantly, the charge density on surface Al atoms increases, while that on O atoms decreases, for both supports. This pattern resembles a back donation mechanism, as reported in previous studies[60,62], where electron density is transferred from O to Al, assisted by the presence of the adsorbed metal species.

The EDD maps in Fig. 5 provide a real-space visualization of these charge redistributions. Regions of charge depletion are observed around Ni and surface O atoms, whereas charge accumulation is localized near Al atoms. The EDD features are in excellent agreement with the Mulliken analysis, confirming that Ni adsorption promotes electron transfer from the dimer to the alumina support and enhances the polarization of the Al-O framework. These results further validate the description of the Ni/α-Al_2O_3 interfaces obtained with the present DFT + U+D2 approach.

CH_4 adsorption

Methane is remarkably stable because of the high C–H bond dissociation energy and its symmetric tetrahedral geometry[63]. Consequently, the first C–H bond cleavage is one of the most energy-demanding elementary steps in dry reforming of methane. Before addressing activation, it is essential to clarify how CH_4 interacts with the different components of the catalyst. For this reason, CH_4 adsorption was first examined on the bare α Al_2O_3(0001) and α Al_2O_3 OH(0001) surfaces, then on the corresponding Ni dimer supported systems. All relevant adsorption sites and molecular orientations were systematically explored, and only the most stable structures are reported in Fig. 6.

On the bare supports, CH_4 is weakly bound to both α Al_2O_3(0001) and α Al_2O_3 OH(0001), with adsorption energies of approximately minus 0.24 eV and minus 0.31 eV, respectively. The optimized geometries show that the CH_4 molecule remains almost perfectly tetrahedral, with C–H bond lengths and H–C–H angles essentially identical to the gas phase values. No elongation of specific C–H bonds is observed, and there is no clear orientation associated with bond activation, such as significant tilting toward a particular surface cation or an O–H group. These features, together with the small adsorption energies, indicate a physisorbed state dominated by dispersion interactions, rather than chemisorption or sizable charge transfer. In other words, the support acts as an almost inert, weakly attractive platform for CH_4, and it does not preactivate the molecule through significant structural distortion[64].

The slightly more exothermic adsorption on the hydroxylated α Al_2O_3 OH(0001) surface, about 0.07 eV more stable than on α Al_2O_3(0001), points to a modest role of surface hydroxyls in strengthening CH_4 binding. Although CH_4 is nonpolar, its electron cloud is polarizable, and the presence of surface O–H groups increases the local heterogeneity of the electrostatic field. This can enhance the induced dipole interaction between CH_4 and the surface and can also lead to a more favorable packing of CH_4 in shallow potential wells created by hydroxyl-rich regions. The absence of any directional hydrogen bonding, which is expected given the lack of a permanent dipole and lone pairs on CH_4, is consistent with this picture. The difference of a few tenths of an electronvolt is small in absolute terms, and of the same order as typical DFT errors for physisorption; however, it is systematic across the different models, which suggests a real physical trend rather than numerical noise.

CH_4 adsorption on the Ni dimer supported systems, Ni/α Al_2O_3(0001) and Ni/α Al_2O_3 OH(0001), was then investigated by considering top, bridge, and interfacial configurations, where CH_4 interacts predominantly with Ni, predominantly with the support, or with both simultaneously. As on the bare alumina surfaces, no single adsorption site clearly emerges as a uniquely preferred minimum. Several structures lie within a very narrow energy window, and the corresponding adsorption energies remain small in magnitude. Importantly, CH_4 does not form any strong σ complex with the Ni dimer; that is, there is no evidence of a configuration where one C–H bond is significantly elongated and directed toward a Ni center. Instead, CH_4 tends to reside at distances characteristic of weak van der Waals interactions, and the molecule often sits in a region where it interacts with both Ni and nearby O atoms without forming any specific bond. This lack of a well-defined, strongly bound molecular adsorption state on Ni might seem counterintuitive if one expects Ni to be the primary site for methane activation. However, it is consistent with previous theoretical and experimental work on CH_4 adsorption on late transition metals and metal oxides[65,66]. Many studies report that intact CH_4 is only weakly bound in the initial state, and that the catalytic role of the metal emerges primarily in the transition state and in the stabilization of

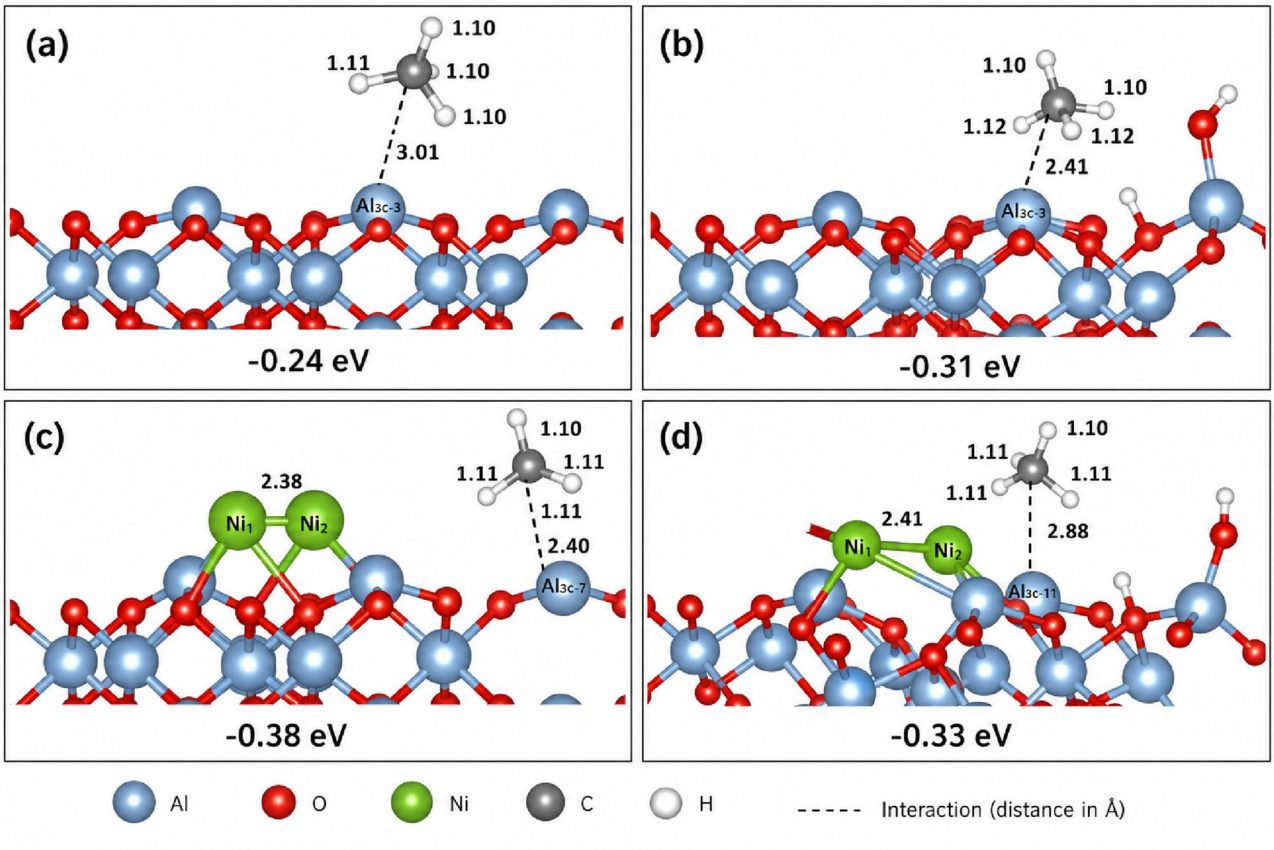


Fig. 6. Optimized geometries of CH_4 adsorbed on (**a**) α Al_2O_3(0001), (**b**) α Al_2O_3 OH(0001), (**c**) Ni/α Al_2O_3(0001) and (**d**) Ni/α Al_2O_3 OH(0001) obtained with the DFT + U+D2 method.

reaction intermediates such as CH_3 and H, rather than in the formation of a deeply bound molecular precursor. In this sense, the calculated adsorption energies and geometries are in line with the broader understanding that strong catalytic activity does not necessarily require strong molecular adsorption of the reactant.

The electron density difference maps in Fig. 7 provide a complementary view of the interaction. For all systems, CH_4 adsorption induces only very modest rearrangements of electron density, localized mainly around the surface atoms and the Ni dimer. There is no significant charge accumulation on the CH_4 molecule and no clear charge transfer channel between CH_4 and either the alumina surface or the Ni dimer. Instead, one observes small polarization effects, where the electronic density around surface O and Ni atoms is slightly shifted in response to the presence of CH_4. This is characteristic of physisorption, and is fully consistent with the negligible structural distortions and the low adsorption energies. The EDD analysis, therefore, reinforces the conclusion that methane adsorption on both alumina and Ni-supported alumina is weak and non-activating.

At this point, it is important to separate two concepts that are sometimes implicitly conflated: adsorption strength and catalytic activity. The present results show that CH_4 is only physisorbed on both the bare and Ni-decorated alumina surfaces, with no evident pre-activation of a specific C–H bond in the adsorbed state. This could be misinterpreted as an indication that Ni is catalytically irrelevant. However, according to the Sabatier principle and modern microkinetic views, what controls reactivity is the balance between binding of intermediates and the height of the activation barriers, not the depth of the initial molecular adsorption well. For a very stable molecule such as CH_4, the decisive step is the formation of the transition state associated with the first C–H bond cleavage. The role of Ni is expected to appear in the lowering of this barrier by providing a favorable environment for the partial transfer of electron density from the C–H bond to the metal and to coadsorbed species. Weak molecular adsorption in the initial state is therefore fully compatible with a strong catalytic effect at the transition state.

Finally, there are some limitations that should be kept in mind when interpreting these adsorption energies. First, the calculations correspond to isolated CH_4 molecules at zero Kelvin and very low coverage, whereas the DRM reaction operates at high temperatures and often under conditions where coadsorption of CO_2, CO, O, OH, or other intermediates on Ni is significant. These coadsorbed species can strongly modify the effective adsorption landscape, for example, by creating new sites for CH_4 activation or by stabilizing partially dehydrogenated intermediates. Second, entropic effects at finite temperature will further weaken physisorbed states, making the already shallow molecular adsorption wells even less populated under realistic conditions. Within this context, the present results should be viewed as a baseline characterization of the intrinsic, low coverage interaction between CH_4 and the clean surfaces. The subsequent analysis of C–H bond activation and dehydrogenation is needed to capture the catalytic role of Ni in DRM fully.

CO_2 adsorption

CO_2 activation is a fundamental step in dry reforming of methane, since CO_2 is the primary oxidizing agent that accepts the oxygen removed from CH_4 and helps prevent carbon deposition[67,68]. Understanding how CO_2 binds and is activated on the different components of the catalyst is therefore essential. In this work, CO_2 adsorption was systematically investigated on the isolated Ni dimer, on the pure and hydroxylated alumina surfaces, and on the Ni-supported α-Al_2O_3 (0001) and α-Al_2O_3 OH(0001) systems. For each model, a broad set of initial positions and orientations of CO_2 was considered, including top, bridge, and interfacial configurations, and the most stable adsorption structures were identified and analyzed to clarify the mechanism of CO_2 activation in DRM.

On the bare α-Al_2O_3 (0001) surface, CO_2 exhibits strong chemisorption. The most stable structure, shown in Fig. 8, has an adsorption energy of −2.08 eV, which indicates a robust interaction between CO_2 and the alumina surface. In this configuration, the carbon atom binds directly to a surface oxygen site (O3c-9) with a C-O3c-9 bond length of 1.36 Å, while the two oxygen atoms of CO_2 coordinate to surface Al atoms (Al3c-3 and Al3c-7) with bond lengths of 1.881 Å and 1.94 Å, respectively.

This bonding pattern corresponds to a carbonate-like species anchored to the surface. Consistently, the O-C-O angle is significantly bent from the linear gas-phase value of 180 degrees to about 125.4 degrees. Such

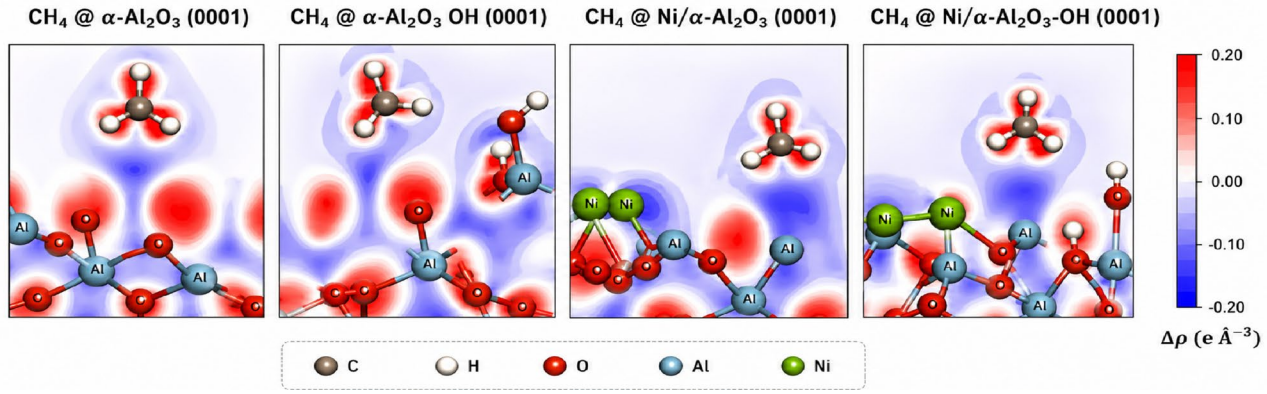


Fig. 7. Electron density difference maps for CH_4 adsorption on the different systems studied.

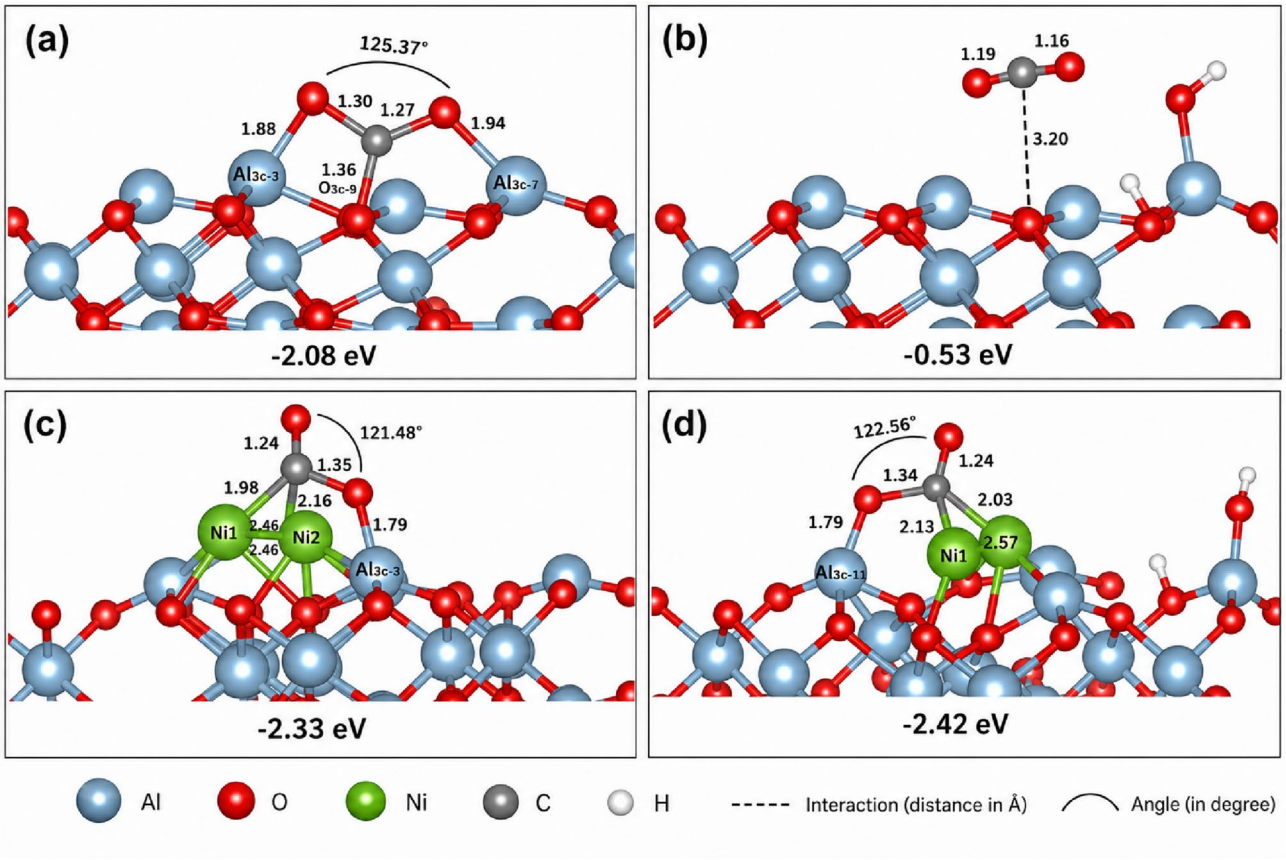


Fig. 8. Optimised geometries of CO_2 adsorbed over (**a**) α-Al_2O_3 (0001), (**b**) α-Al_2O_3-OH (0001), (**c**) Ni/α-Al_2O_3(0001), and (**d**) Ni/α-Al_2O_3-OH (0001) using the DFT + U+D2 method.

a large deviation from linearity is a clear signature of strong activation of CO_2, in line with the chemisorbed carbonate structures reported experimentally and theoretically by Casarin et al.[69]. In other words, the α Al_2O_3(0001) surface alone is able to strongly bind and deform CO_2, already providing a first level of activation relevant for DRM.

The situation is markedly different on the hydroxylated α Al_2O_3 OH(0001) surface. Here, the most stable configuration has an adsorption energy of only − 0.53 eV, which is much less exothermic than on the pure alumina surface. The optimized geometry shows CO_2 lying nearly parallel to the surface in a hollow site, without forming specific short bonds to individual surface atoms. Importantly, the molecule retains an almost linear O-C-O angle, and the internal C-O bond lengths remain close to their gas-phase values. This indicates that the interaction is largely physical and that CO_2 is not substantially activated on the hydroxylated surface. The presence of hydroxyl groups evidently passivates some of the Lewis acid and base sites of alumina and suppresses the formation of strongly chemisorbed carbonate species. From an electronic point of view, this passivation can be rationalized as follows. On the clean α-Al_2O_3(0001) surface, the three-coordinated Al^{3+} cations (Al3c) expose empty 3sp-derived states that lie just above the Fermi level and act as strong Lewis acid sites able to accept electron density from incoming CO_2 molecules, while the two-coordinated O^{2-} anions (O2c) carry localized 2p lone pairs that act as Lewis base sites and can donate density into the CO_2 π^* orbitals. Upon hydroxylation, an OH group binds to the Al3c cation, filling its acceptor states with hybridized O–H bonding orbitals, while the surface O2c sites are protonated to OH and the resulting σ(O–H) and lone-pair orbitals lie deeper in the valence band, well below the Fermi level. The empty Al-derived states are therefore largely removed from the frontier region, and the basic O lone pairs are stabilized and made less available for donation. The net effect is a quenching of the donor–acceptor pair that drives CO_2 activation on the bare surface, which is consistent with the substantial reduction of charge transfer to CO_2 and the loss of bending and chemisorption on the hydroxylated model. This contrast between pure and hydroxylated alumina highlights a key role of surface hydroxylation in tuning CO_2 activation: while hydroxyls can improve CH_4 physisorption slightly, they strongly weaken CO_2 chemisorption.

For the Ni-supported catalysts, Ni/α Al_2O_3(0001) and Ni/α Al_2O_3 OH(0001), the most stable CO_2 adsorption structures (Fig. 8) correspond to interfacial geometries where CO_2 interacts simultaneously with Ni and the alumina support. On Ni/α Al_2O_3(0001), the carbon atom coordinates to both Ni atoms of the dimer, with C-Ni1 and C-Ni2 distances of 1.98 Å and 2.17 Å, respectively, while one oxygen atom binds to Al3c-3 with a bond length of 1.79 Å. This creates a three-center arrangement involving Ni, C and Al, reminiscent of a metal supported carbonate or carboxylate-like intermediate. On Ni/α Al_2O_3 OH(0001), the carbon atom again binds

to both Ni atoms, with C-Ni distances of 2.13 Å and 2.03 Å, while one oxygen atom is bonded to Al3c-11 at 1.79 Å. The O-C-O angles are reduced to 121.5 degrees and 122.6 degrees for Ni/α Al_2O_3(0001) and Ni/α Al_2O_3 OH(0001), respectively, which indicates even stronger bending and activation of CO_2 than on the pure alumina surface. The corresponding adsorption energies of −2.33 eV and − 2.42 eV are more negative than on bare α Al_2O_3(0001), confirming that the presence of Ni at the interface further stabilizes and activates CO_2. These geometric and energetic trends are consistent with the partial density of states (PDOS) analysis. For CO_2 on α Al_2O_3(0001), the PDOS shows a clear overlap between the s and p states of the CO_2 atoms (C, O1, and O2) and the surface O3c-9 and Al3c-3/Al3c-7 states around the Fermi level (Figure S1(a)). This indicates significant orbital mixing and explains the strong chemisorption and pronounced bending. In contrast, on the hydroxylated α Al_2O_3 OH(0001) surface, the interaction is weaker and more diffuse, consistent with the lower adsorption energy and the preservation of the linear geometry.

For the Ni-supported systems, the PDOS of Ni/α Al_2O_3(0001) and Ni/α Al_2O_3 OH(0001) (Figures S1(b) and S1(c)) reveals strong hybridisation between the Ni d states and the C and O states of CO_2, as well as between CO_2 and the Al3c-3 or Al3c-11 surface atoms. The appearance of intense superposition peaks indicates the formation of new bonding and antibonding states that involve both Ni and surface Al sites. This hybridisation rationalizes the very negative adsorption energies and the strong bending of CO_2, and it underlines the cooperative role of the metal-support interface: CO_2 is not simply bound to Ni or to alumina alone, but rather to a Ni-Al-O ensemble that provides an efficient activation environment.

The Mulliken charge analysis offers a complementary picture of this activation. As summarized in Table 3, the net charge on CO_2 becomes increasingly negative upon adsorption: about − 0.57 e on α Al_2O_3(0001), and approximately − 1.04 e and − 1.02 e on Ni/α Al_2O_3(0001) and Ni/α Al_2O_3 OH(0001), respectively.

This indicates substantial electron transfer from the catalyst to the adsorbed CO_2, especially in the presence of Ni. In the supported systems, the Ni dimer itself becomes more positively charged after adsorption, its net charge increasing from + 0.36 e (clean Ni/α Al_2O_3(0001)) to + 1.02 e and from + 0.52 e (clean Ni/α Al_2O_3 OH(0001)) to + 1.12 e. At the same time, the Al atoms involved in the interface, in particular Al3c-3 and Al3c-11, also become more positive. In contrast, nearby O atoms become slightly less negative or remain strongly negative, depending on their involvement in the bonding network. This pattern shows that the surface Al-O framework and the Ni dimer act together as charge donors, while CO_2 acts as a strong charge acceptor.

Overall, the charge analysis reveals a clear Al(donor) - Ni - CO_2(acceptor) synergy. The alumina surface helps polarize and stabilize the Ni dimer, which in turn enhances electron donation to CO_2. This cooperative effect explains why CO_2 adsorption is even stronger on the Ni-supported systems than on bare alumina, despite the somewhat passivating effect of hydroxyl groups on the support. It also indicates that the most active sites for CO_2 activation are located at the metal-support interface, rather than on Ni or alumina alone.

The electron density difference (EDD) maps in Fig. 9 visualize these charge redistribution processes in real space. For all strongly adsorbed configurations, the EDD maps show charge accumulation around the carbon and oxygen atoms of CO_2 and charge depletion on the neighboring Ni, Al and O atoms on the surface.

This confirms that CO_2 behaves as a strong electron acceptor, forming activated, partially reduced species on the surface. The qualitative agreement between the EDD patterns and the Mulliken charges strengthens the conclusion that charge transfer from the Ni alumina substrate to CO_2 is a key factor in stabilizing and activating the adsorbed molecule.

From a catalytic standpoint, these results highlight a sharp contrast between CH_4 and CO_2. While CH_4 is only weakly physisorbed with negligible structural distortion, CO_2 can form strongly chemisorbed, bent species, especially at the Ni alumina interface. This means that under DRM conditions, CO_2 is more easily activated than CH_4, and that the catalyst will tend to accumulate CO_2-derived surface intermediates, such as carbonate

	α-Al_2O_3 (0001)		Ni/α-Al_2O_3 (0001)		Ni/α-Al_2O_3-OH (0001)	
	Before	**After**	**Before**	**After**	**Before**	**After**
CO_2	0.00	−0.57	0.00	−1.04	-	−1.02
Ni_2	-	-	0.36	1.02	-	1.12
Oxygen						
O_{3c1}	-	-	-	−1.07	-	−1.10
O_{3c2}	-	-	-	−1.07	-	-
O_{3c21}	-	-	-	−1.07	-	−1.05
O_{3c25}	-	-	-	-	-	−1.05
O_{3c8}	-	-	-	−1.06	-	-
O_{3c9}	−1.14	−0.78	-	-	-	-
Aluminum						
Al_{3c3}	-	-	1.56	1.82	-	1.82
Al_{3c7}	1.78	1.85	-	-	-	-
Al_{3c9}	1.78	1.92	-	-	-	-
Al_{3c11}	-	-	-	1.44	-	1.29

Table 3. Mulliken Charges (e) for CO_2 adsorbed on α-Al_2O_3 surfaces and Ni-supported systems.

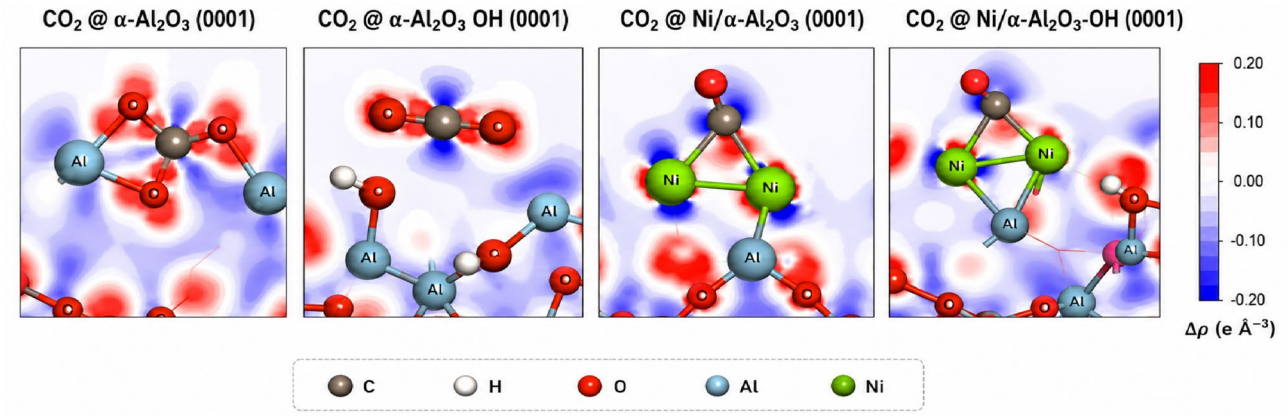


Fig. 9. EDD map for CO_2 adsorption on the different studied systems.

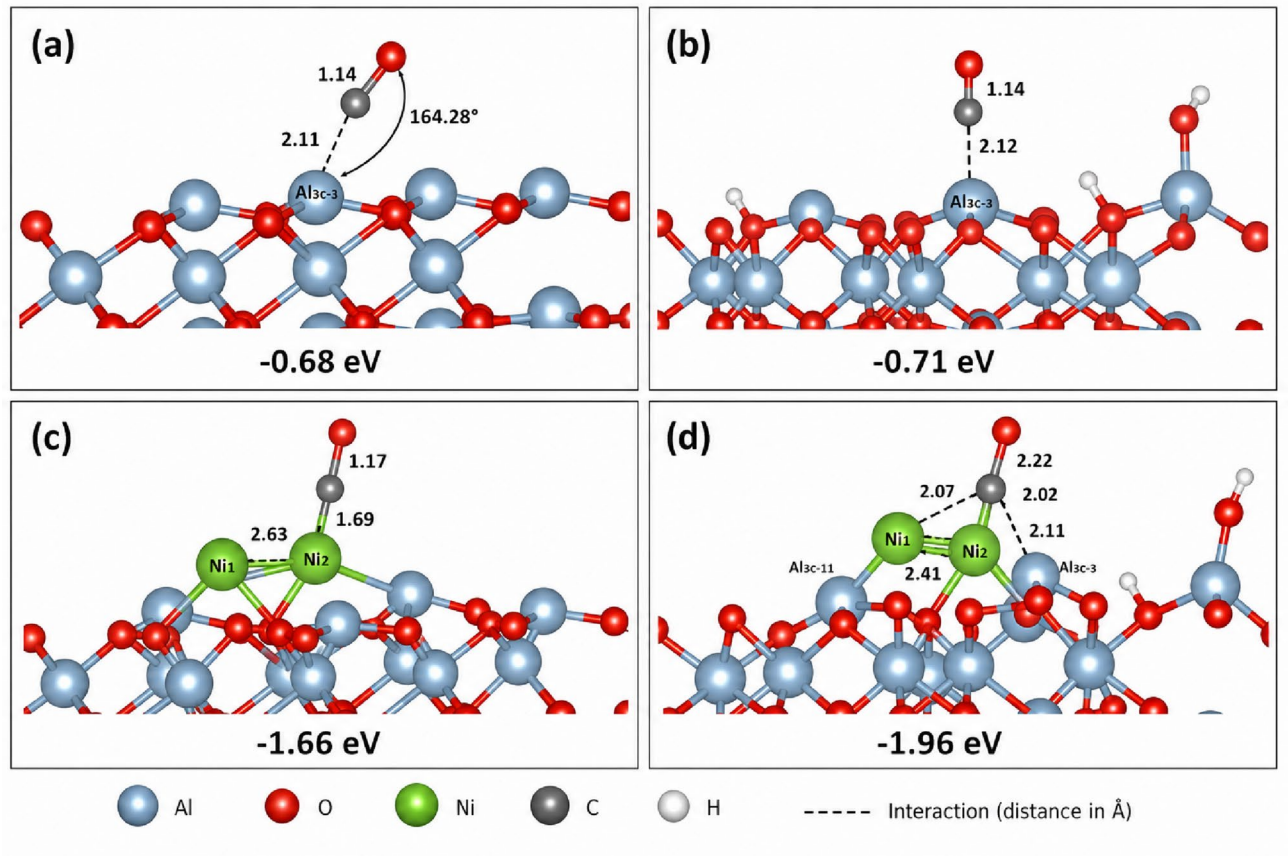


Fig. 10. Optimised Geometries of CO Adsorption on (**a**) α-Al_2O_3(0001), (**b**) α-Al_2O_3-OH (0001), (**c**) Ni/α-Al_2O_3 (0001), and (**d**) Ni/α-Al_2O_3-OH (0001) Using the DFT + U+D2 Method.

or carboxylate species, at the metal-support perimeter. These activated CO_2 species can then participate in subsequent steps, for example, in oxidizing surface carbon and CHx fragments produced during methane dehydrogenation. The strong CO_2 activation at the Ni alumina interface is therefore expected to play a central role in balancing carbon formation and removal and in maintaining catalyst stability during DRM.

CO adsorption

All possible configurations for CO adsorption on the modeled surfaces were examined. For the α Al_2O_3(0001) and α Al_2O_3 OH(0001) supports, the most stable structures, shown in Fig. 10(a, b), reveal that CO remains essentially linear and its internal C O bond length is virtually unchanged with respect to the gas phase value. The molecule resides above surface sites at distances typical of weak interactions and no short C O_surface or

C Al contacts are formed. The corresponding adsorption energies are modest, −0.68 eV on α Al_2O_3(0001) and −0.71 eV on α Al_2O_3 OH(0001). These values, together with the negligible structural changes, indicate purely physical adsorption, dominated by dispersion and weak electrostatic interactions. This conclusion is consistent with the experimental results of Rohmann et al.[70], who reported a weak interaction of CO with α Al_2O_3(0001), with an adsorption energy of about − 0.52 eV, confirming that clean alumina surfaces are essentially inert toward CO in both theory and experiment.

On the Ni supported systems Ni/α Al_2O_3(0001) and Ni/α Al_2O_3 OH(0001), the picture changes qualitatively, see Fig. 10(c, d). For Ni/α Al_2O_3(0001), CO adsorbs in the classical atop configuration, with the C atom bound to a Ni site (Ni2) and a C Ni bond length of 1.69 Å. The C O distance is slightly elongated, from 1.15 Å in the gas phase to 1.17 Å in the adsorbed state, which indicates a moderate activation of the CO bond, typical of a Blyholder-type σ donation and π back donation interaction between CO and a late transition metal. The adsorption energy of −1.66 eV reflects a strong chemisorption state, substantially more exothermic than on bare alumina, and comparable in magnitude to values reported on Ni surfaces in the literature.

On Ni/α Al_2O_3 OH(0001), the preferred adsorption geometry is an interfacial configuration rather than a simple atop site. The carbon atom interacts simultaneously with both Ni atoms and with the surface Al3c 3 atom, leading to a three-center arrangement. The C Ni1, C Ni2, and C Al3c 3 distances are 2.10, 2.02, and 2.10 Å, respectively, while the C O bond is dramatically elongated to 2.22 Å. Such a large elongation goes far beyond the moderate activation seen on Ni/α Al_2O_3(0001). It suggests that the C O bond is almost completely broken, so that CO behaves more like a pair of strongly bound C and O fragments coordinated to the metal support ensemble than like an intact molecule. The adsorption energy in this case is −1.96 eV, more negative than on Ni/α Al_2O_3(0001), which confirms that the hydroxylated interface stabilises an even more activated, almost dissociated CO state.

The projected density of states, PDOS, provides a microscopic explanation for these trends. For CO on Ni/α Al_2O_3(0001), Figure S2(a) shows pronounced overlap between the Ni2 3 d states and the C 2p states in an energy window extending from about − 9.4 to 5 eV, together with hybridisation between Ni2 s and C s states over lower and higher energy ranges. This pattern is consistent with the classical picture of CO binding on late transition metals, where CO donates electron density from its 5σ orbital into empty metal states and receives back donation from filled metal d states into its 2π* antibonding orbital. The modest C O elongation and the strong adsorption energy fit this Blyholder-type mechanism.

For CO on Ni/α Al_2O_3 OH(0001), Figure S2(b) reveals even more extensive hybridisation. Both Ni atoms contribute 3 d and s states that strongly overlap with the C 2p and s states, and the Al3c 3 states also participate in the bonding manifold. In other words, the CO-derived species is not simply bound to a single Ni atom, but is electronically coupled to a multi-centre Ni Ni Al environment at the metal support perimeter. The large C O bond elongation and the more exothermic adsorption energy reflect the formation of new C centred states that mix strongly with the Ni d band and disrupt the internal CO bonding. This multi centre interaction is a direct consequence of the hydroxylated interface geometry and underlines the special role of the perimeter region, rather than flat Ni sites, in controlling CO activation.

Mulliken charge analysis supports this interpretation. As reported in Table 4, the net charge on CO changes from 0.00 e in the gas phase to about − 0.22 e on Ni/α Al_2O_3(0001), and to −0.68 e on Ni/α Al_2O_3 OH(0001).

At the same time, the Ni dimer becomes significantly more positive. Its total charge increases from + 0.36 e to + 0.58 e on Ni/α Al_2O_3(0001) and from + 0.52 e to + 1.00 e on Ni/α Al_2O_3 OH(0001) after CO adsorption. These changes clearly indicate substantial electron transfer from Ni to CO, especially on the hydroxylated interface. The larger negative charge on CO on Ni/α Al_2O_3 OH(0001) correlates directly with the stronger adsorption and the almost complete C O bond cleavage, confirming that charge transfer and back donation are key to the enhanced activation at the hydroxylated perimeter. The changes in Al charges, particularly the increase in positive character of Al3c 3 when it enters the bonding network, also show that the alumina cation participates in the electron redistribution, and that the interface behaves as a cooperative Ni Al donor rather than as isolated Ni atoms on an inert support.

	Ni/α-Al_2O_3(0001)		Ni/α-Al_2O_3-OH (0001)	
	Before	**After**	**Before**	**After**
CO	0.00	−0.22	0.00	−0.68
N_2	0.36	0.58	0.52	1.00
Oxygen				
O_{3c1}	−1.09	−1.07	-	-
O_{3c2}	−1.08	−1.07	-	-
O_{3c21}	−1.09	−1.05	−1.08	−1.08
O_{3c8}	−1.06	−1.05	−1.06	−1.05
Aluminium				
Al_{3c11}	1.41	1.34	1.46	1.11
Al_{3c15}	1.66	1.52	-	-
Al_{3c3}	-	-	1.29	1.62

Table 4. Mulliken Charges for CO before and after adsorption on Ni-supported alumina systems.

The electron density difference, EDD, maps in Fig. 11 visualise these charge redistribution processes in real space. For CO on Ni/α Al_2O_3(0001), the EDD shows clear charge depletion around the Ni site and charge accumulation along the C O axis, mainly near the C atom, which is exactly what one expects from donation and back donation between Ni and CO. On Ni/α Al_2O_3 OH(0001), the depletion lobes on both Ni atoms and on Al3c 3 are more pronounced, and the accumulation near the C centred region is stronger and more extended.

This is consistent with a larger transfer of electron density into CO derived antibonding states and further supports the idea that the C O bond is heavily weakened or effectively broken at the interface. In sharp contrast, the EDD maps for CO on α Al_2O_3(0001) and α Al_2O_3 OH(0001) show only very small, diffuse polarization around surface atoms and no clear accumulation on CO, in line with the weak physisorption concluded from energies and geometry.

From a catalytic perspective, these findings have several implications. First, they confirm that clean alumina plays almost no direct role in CO activation: CO is only weakly physisorbed and remains essentially inert on α Al_2O_3, regardless of hydroxylation. Second, they demonstrate that Ni sites and, more specifically, Ni sites at the metal support interface are responsible for strong CO adsorption and activation. On flat Ni atop sites, as represented by Ni/α Al_2O_3(0001), CO is strongly bound but still largely molecular, so it can act as a reversible spectator or intermediate. At the hydroxylated Ni alumina perimeter, Ni/α Al_2O_3 OH(0001), CO becomes much more strongly activated and can approach dissociation, which is beneficial for some oxidation pathways but also increases the risk of forming tightly bound carbonaceous residues if oxygen is insufficient.

Third, when these CO results are interpreted together with the CH_4, CO_2, H_2 and C adsorption data (the H_2 and C adsorption analyses are presented in detail in Sect. 3.5 and 3.6, respectively), a coherent pattern emerges. CH_4 and H_2 remain weakly bound and are not significantly activated in the molecular state, CO_2 and CO are strongly activated at Ni alumina interfaces, and atomic C is very strongly stabilised in the same regions. The strong CO binding and activation at the perimeter indicate that CO can act as both a reaction intermediate and a potential poison, competing with other adsorbates for Ni sites. The fact that hydroxylation strengthens CO and C binding, while also helping CO_2 activation, implies that the hydroxylated interface is a highly reactive but also potentially coke prone region. Whether this reactivity leads to improved carbon removal or to faster deactivation will depend on the balance between CO and CO_2 availability, oxygen coverage and the kinetics of C oxidation steps, which are beyond the scope of the present adsorption based study but are clearly constrained by the strong interfacial interactions identified here.

Overall, the CO adsorption analysis confirms the crucial role of Ni and the Ni alumina interface in binding and activating carbon monoxide, while highlighting the relative inertness of the bare alumina surfaces. It also shows that hydroxylation does not simply introduce weak hydrogen bonding sites, but profoundly modifies the interfacial electronic structure, strengthening electron donation to CO and promoting near dissociation of the C O bond at the perimeter.

H_2 adsorption

The formation of H_2 is a pivotal step in the DRM process, since H_2 is a main product and its desorption controls part of the catalytic turnover[71]. To clarify how H_2 interacts with the different components of the catalyst, H_2 adsorption was systematically investigated on α Al_2O_3(0001) and α Al_2O_3 OH(0001), as well as on the corresponding Ni supported systems, Ni/α Al_2O_3(0001) and Ni/α Al_2O_3 OH(0001). For each model, several initial configurations were considered, including planar and perpendicular orientations of H_2 and positions above Al and O sites, above the Ni dimer and at the metal support interface. Figure 12 presents the optimized geometries of the most stable adsorption structures together with the key geometric parameters. On the bare alumina surfaces, H_2 preferentially adopts a planar configuration above an Al3c 3 site on both α Al_2O_3(0001) and α Al_2O_3 OH(0001). The distances between the molecular center of H_2 and the surface are 2.16 Å for the pure surface and 2.07 Å for the hydroxylated one. The corresponding adsorption energies are minus 0.20 eV and minus 0.21 eV, respectively. These small exothermic values indicate weak physisorption driven primarily by dispersion forces. Importantly, the H H bond length and the internal geometry of the molecule remain

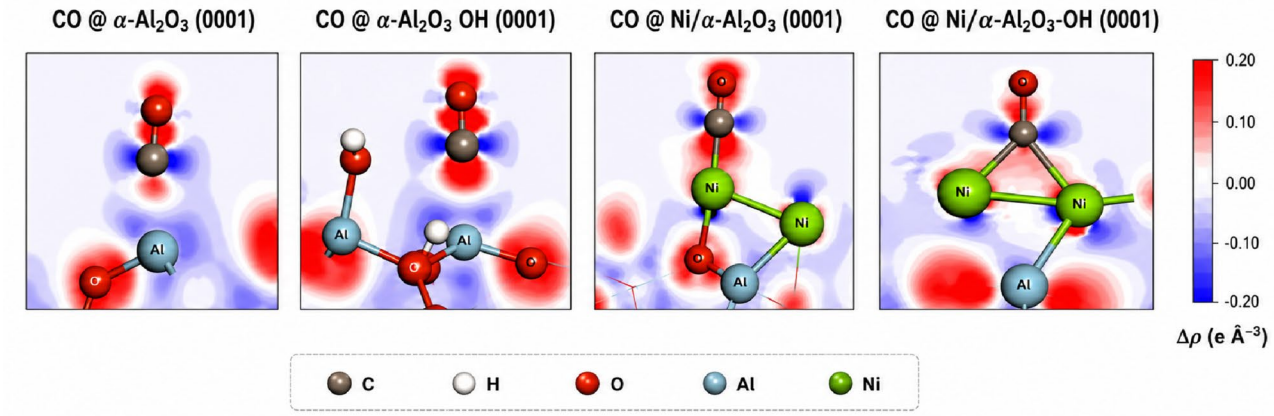


Fig. 11. EDD map for CO adsorption on the different studied systems.

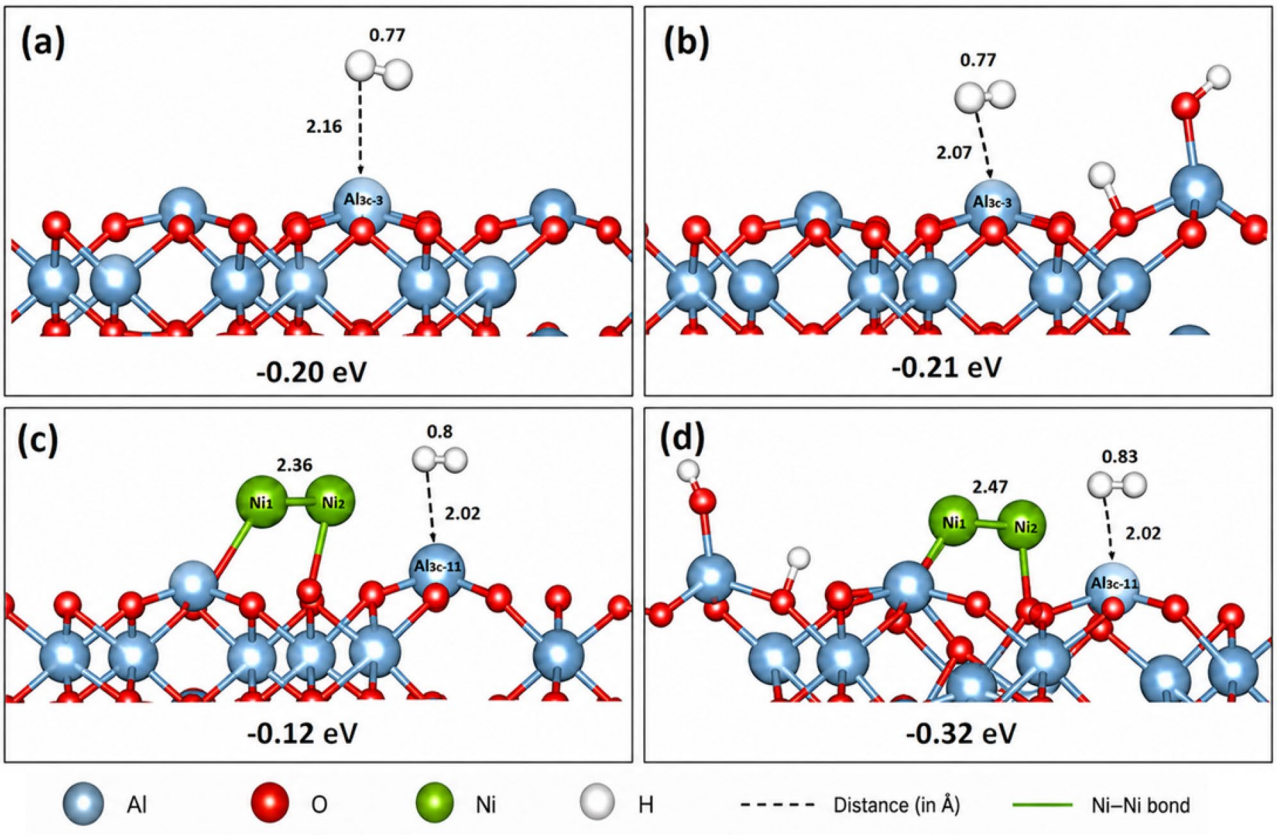


Fig. 12. Optimized geometries of H_2 adsorbed on (**a**) α Al_2O_3(0001), (**b**) α Al_2O_3 OH(0001), (**c**) Ni/α Al_2O_3(0001) and (**d**) Ni/α Al_2O_3 OH(0001) obtained with the DFT + U+D2 method.

essentially unchanged compared with the gas phase. There is no evidence of bond elongation or asymmetric distortion that would indicate partial activation toward dissociation. The very similar adsorption energies on the two surfaces also show that hydroxylation has only a marginal effect on molecular H_2 binding. In other words, alumina behaves as a largely inert support for H_2, despite its stronger interactions with CO_2.

For the Ni supported catalysts, an extensive search was carried out including adsorption sites directly on top of Ni, bridging between the two Ni atoms and at various positions near the metal support perimeter. After full relaxation, in all cases H_2 migrated away from the Ni dimer and stabilized above an Al site of the support in a planar orientation. This behavior is observed on both Ni/α Al_2O_3(0001) and Ni/α Al_2O_3 OH(0001) and it clearly indicates that the molecular H_2 state does not form a stable σ complex with Ni under the conditions modeled. Instead, the preferred adsorption sites remain on the alumina lattice, even in the presence of Ni. The equilibrium distances between H_2 and the surface are 2.02 Å for Ni/α Al_2O_3(0001) and 1.93 Å for Ni/α Al_2O_3 OH(0001), slightly shorter than on the corresponding bare supports but still typical for weak physical adsorption.

The calculated adsorption energies on the Ni supported systems are minus 0.12 eV for Ni/α Al_2O_3(0001) and plus 0.32 eV for Ni/α Al_2O_3 OH(0001). The first value corresponds to very weak physisorption that is even less favorable than on bare alumina. The positive value of 0.32 eV means that there is no thermodynamically stable molecular adsorption well on the hydroxylated Ni supported surface, the gas phase state is actually lower in energy. At this point, it is important not to overinterpret small differences. Energies of the order of a few tenths of an electronvolt are within the typical uncertainty of DFT for weakly bound states, especially when dispersion corrections are involved. What is robust is the qualitative conclusion, H_2 does not chemisorb or dissociate spontaneously on any of these models and, whenever a bound state exists, it is purely physisorbed and relatively shallow. The finer distinction between minus 0.20, minus 0.12 or minus 0.21 eV should not be treated as a precisely tunable trend, but rather as variations within a consistently weak interaction regime.

These trends are consistent with the Mulliken charge analysis. For all systems, the net charge on H_2 remains essentially zero, with no significant charge transfer from the alumina surface or from the Ni dimer to the molecule. This is in strong contrast to CO_2, for which the calculated charges show substantial electron uptake upon adsorption. The electron density difference maps in Fig. 13 confirm this picture.

They reveal only very small, localized polarization of the electron density around surface Al and O atoms near the adsorbed H_2, and no obvious charge accumulation on the molecule itself. There are no features reminiscent of metal hydride formation or of a transition toward dissociative adsorption. The EDD analysis therefore reinforces the interpretation that, whenever H_2 is bound, the interaction is purely physical and non activating. From a mechanistic viewpoint, these results carry several important implications and some of them

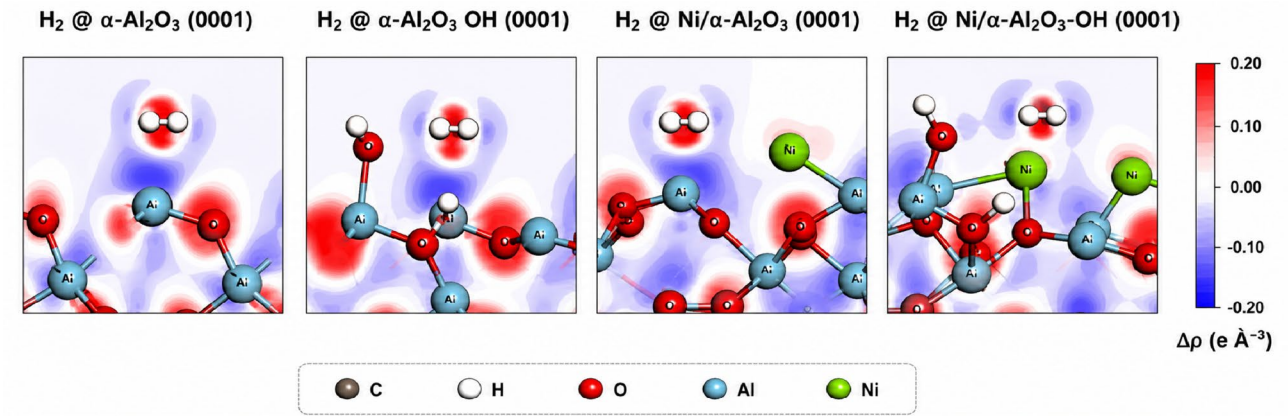


Fig. 13. Electron density difference maps for H_2 adsorption on the different systems studied.

run counter to naive expectations. First, alumina plays almost no direct role in stabilizing molecular H_2, despite its strong ability to chemisorb and bend CO_2. The same support that provides strongly activated carbonate-like species from CO_2 only provides weak physisorption wells for H_2. This difference is important for DRM, since it suggests that the support is more relevant for oxidizing carbonaceous intermediates through activated CO_2 species than for controlling H_2 binding. Second, the presence of Ni, at least in the form of a small dimer, does not improve molecular H_2 adsorption. In fact, in the present models H_2 actively avoids the Ni dimer in the relaxed structures and chooses to sit over alumina.

This can look paradoxical if one expects Ni to be the primary site for H_2 chemistry. The resolution is that Ni is not needed to stabilize molecular H_2, it is needed to stabilize and recombine adsorbed H atoms. In other words, the catalytic relevance of Ni manifests at the level of dissociative adsorption and H H recombination barriers, not at the level of weak molecular adsorption. This is in line with Zhang et al.[72] and with many studies on H_2 on late transition metals, where the important quantity is the barrier between H and H_2 states rather than the depth of the molecular H_2 well. Third, when comparing CH_4, CO_2 and H_2, a consistent picture emerges. CH_4 is only weakly physisorbed and not pre activated on either alumina or Ni supported alumina. CO_2 is strongly chemisorbed and bent on α Al_2O_3(0001) and even more strongly activated at the Ni alumina interface. H_2, finally, is only weakly bound and often prefers to remain in the gas phase. So the catalyst, and especially the metal support perimeter, is very effective in activating CO_2, moderately effective in activating CH_4 in the transition states for C H cleavage, but largely indifferent to molecular H_2. This is exactly what one would want for an efficient DRM catalyst, CO_2 should be reactive enough to remove surface carbon, CH_4 should be activated but not overbound, and H_2 should desorb easily once formed.

There are, however, limitations that should be explicitly acknowledged in the discussion for intellectual honesty. All these adsorption energies are calculated at zero Kelvin and very low coverage. Under real DRM conditions, high temperature and significant surface coverage by O, OH, CO, CO_2 derived species and CHx intermediates will modify the effective adsorption landscape. Entropic contributions will further destabilize weakly physisorbed H_2, making the already shallow wells practically irrelevant. In this sense, these results should be interpreted as intrinsic low coverage tendencies rather than quantitative adsorption energies that can be directly compared to high temperature experiments. The qualitative message is robust, H_2 does not form strongly bound molecular intermediates and desorbs easily, but it is misleading to treat a difference of 0.08 or 0.09 eV as a precise descriptor of support effects.

Overall, the combination of adsorption energies, geometry, Mulliken charges and EDD maps leads to a clear conclusion. H_2 interacts only weakly, or not at all, with both alumina and Ni supported alumina in its molecular form. The catalyst therefore promotes H_2 formation not by stabilizing molecular H_2, but by providing suitable adsorption sites and low barriers for surface H formation, migration and recombination. This interpretation is consistent with the CH_4 and CO_2 results and with the broader mechanistic picture of DRM on Ni based catalysts.

C adsorption

Carbon deposition on catalyst surfaces is commonly attributed to methane cracking, which proceeds through successive dehydrogenation steps of CH_4, ultimately yielding surface carbon species that can nucleate and grow into extended carbon structures[73,74]. The Boudouard reaction, that is, CO disproportionation to CO_2 and C, is also recognized as an important pathway to coke formation under certain conditions[75,76]. Both mechanisms can lead to blocking of active sites and progressive catalyst deactivation. In addition, more complex routes, such as surface coupling of CHx intermediates and bulk carbon dissolution followed by segregation, have been proposed to rationalize the rich phenomenology of carbon formation on transition metal catalysts[77].

Recent DFT studies have shown that the propensity for carbon deposition is intimately linked to the detailed pathway of C H bond oxidation and to the activation barriers for CO dissociation and CO oxidation[78]. In other words, carbon deposition is not just a question of thermodynamic stability of surface C, but also of how easily carbon can be removed or converted under reaction conditions. To examine this problem on the present Ni alumina systems, we analyzed the adsorption of an isolated C atom on α Al_2O_3(0001), α Al_2O_3 OH(0001), Ni/α

Al_2O_3(0001) and Ni/α Al_2O_3 OH(0001). The most stable adsorption geometries for each model are shown in Fig. 14, and their electronic structure is discussed in light of PDOS, Mulliken charge and EDD results. On the bare α Al_2O_3(0001) surface, the C atom prefers a bridge site between Al3c 3 and O3c 9. In this configuration, it forms C Al and C O bonds of 2.10 Å and 1.32 Å, respectively, with an adsorption energy of minus 3.54 eV. This large exothermic value indicates a strong chemisorption of carbon on the alumina surface, with clear covalent character in the C O bond and substantial polarization of the local environment. On the hydroxylated α Al_2O_3 OH(0001) surface, the minimum energy configuration is again a bridge site, this time between Al3c 3 and O3c 22, with very similar bond lengths (2.11 Å for C Al3c 3 and 1.32 Å for C O3c 22). The adsorption energy is minus 4.41 eV, significantly more negative than on the non hydroxylated surface. This shows that hydroxylation enhances the thermodynamic stability of adsorbed C on alumina, in sharp contrast to the case of molecular CO_2, where hydroxyls weaken chemisorption. In other words, hydroxyl groups do not universally increase adsorption; they selectively stabilize some species, such as atomic carbon, while passivating sites for others, such as CO_2.

On the Ni supported α Al_2O_3(0001) system, the carbon atom strongly prefers to bind directly to the Ni dimer rather than to the support. The most stable configuration corresponds to a bridge site between Ni1 and Ni2, with C Ni bond distances of 1.98 Å and 2.12 Å. The associated adsorption energy is minus 6.22 eV, which is substantially more exothermic than on the bare alumina supports. This very strong binding reflects the well known tendency of Ni to stabilize carbonaceous species, a key microscopic reason for the high coking sensitivity of Ni based DRM catalysts. On the Ni/α Al_2O_3 OH(0001) system, the most stable carbon configuration is located at the metal support interface, where the C atom simultaneously binds to both Ni atoms and to Al3c 3, with bond lengths of 1.75, 1.88 and 2.01 Å, respectively. The corresponding adsorption energy is minus 6.47 eV, which is the most exothermic value obtained for atomic carbon among all the systems considered in this work. The shorter C–Ni bonds and the additional C–Al interaction confirm that the interface provides an even more favorable electronic environment for C stabilization compared to the pure Ni dimer site. The fact that the preferred site migrates from a pure Ni bridge to a Ni Al interface upon hydroxylation highlights again the cooperative role of the metal support perimeter in trapping carbon.

The PDOS analysis clarifies the nature of these strong interactions. For C on α Al_2O_3(0001) and α Al_2O_3 OH(0001), the PDOS shows a pronounced overlap between the C s and p orbitals and the s and p orbitals of surface O and Al3c 3 atoms (Figure S3(a, b)). This indicates the formation of covalent C O and C Al bonds that induce substantial rearrangement of the valence band states of alumina. In particular, new states appear in the band gap region, which is consistent with the strong chemisorption and the large adsorption energies. For carbon adsorption on Ni supported systems (Figure S3(c, d)), the overlap becomes even more intense. The C s and p states strongly hybridize with the Ni s and d states, and also interact with the neighboring Al orbitals. This

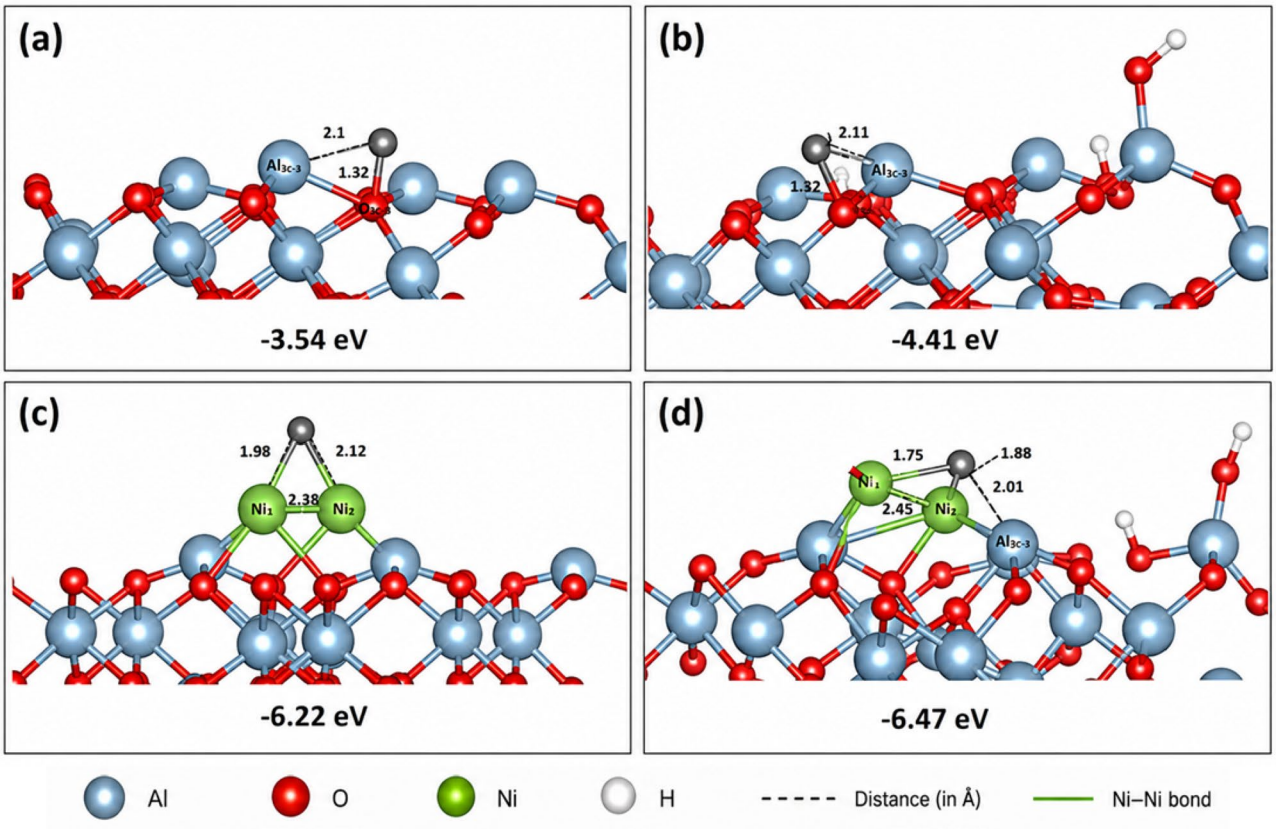


Fig. 14. Optimized geometries of C atom adsorbed over (**a**) α-Al_2O_3(0001), (**b**) α-Al_2O_3-OH (0001), (**c**) Ni/α-Al_2O_3(0001), and (**d**) Ni/α-Al_2O_3-OH(0001) using DFT + U+D2 method.

	α-Al_2O_3 (0001)		α-Al_2O_3-OH (0001)		Ni/α-Al_2O_3 (0001)		Ni/α-Al_2O_3-OH (0001)	
	Before	**After**	**Before**	**After**	**Before**	**After**	**Before**	**After**
C	0.00	−0.19	0.00	−0.19	0.00	−0.57	0.00	−0.8
N_2	-	-	-	-	0.36	0.76	0.52	1.04
Oxygen								
O_{3c1}	−1.14	-	-	-	-	-	-	−1.14
O_{3c2}	-	-	-	−1.08	−1.09	-	−1.08	-
O_{3c8}	-	-	-	-	−1.09	-	-	-
O_{3c9}	−0.7	-	−1.14	-	-	-	-	−0.7
O_{3c14}	-	-	−0.7	-	-	-	-	-
O_{3c21}	-	-	-	-	−1.06	-	−1.08	-
O_{3c25}	-	-	-	-	-	-	−1.01	-
Aluminum								
Al_{3c11}	-	-	-	1.41	1.46	-	1.4	-
Al_{3c3}	1.63	-	1.65	-	-	-	1.56	1.63

Table 5. Mulliken Charges (e) for the C atom before and after adsorbed on α-Al_2O_3(0001) Ni-supported alumina systems.

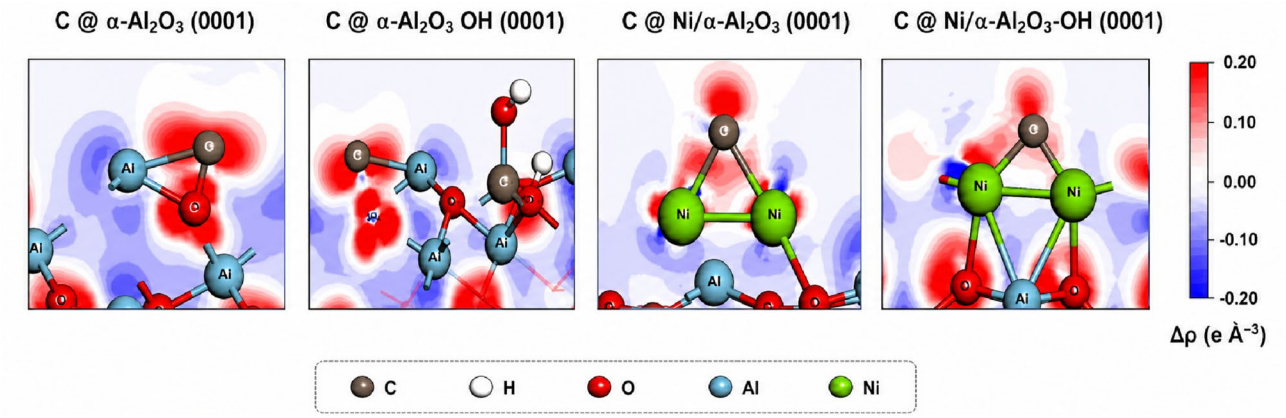


Fig. 15. EDD map for C adsorption on the different studied systems.

leads to broad superposition peaks spanning the Fermi level region, a hallmark of robust metal carbon bonding. The PDOS thus confirms that carbon is more strongly bound on Ni and at the Ni alumina interface than on alumina alone, in agreement with the energetic trends.

The Mulliken charge analysis in Table 5 provides additional insight into the direction of charge transfer. For all models, the C atom becomes negatively charged upon adsorption, with net charges of about minus 0.19 e on α Al_2O_3(0001) and α Al_2O_3 OH(0001), and more negative values of minus 0.57 e and minus 0.80 e on Ni/α Al_2O_3(0001) and Ni/α Al_2O_3 OH(0001), respectively.

At the same time, the Ni dimer becomes significantly more positive: its total charge increases from 0.36 e to 0.76 e on Ni/α Al_2O_3(0001) and from 0.52 e to 1.04 e on Ni/α Al_2O_3 OH(0001). These changes indicate substantial electron donation from the Ni atoms and, to a lesser extent, from the Al O framework to the adsorbed carbon, which behaves as a strong electron acceptor. The more negative charge on C and more positive Ni on the hydroxylated system suggest that the presence of hydroxyl groups further polarizes the interface and enhances charge transfer to the carbon atom. The EDD maps in Fig. 15 visualize this charge redistribution in real space. For all systems, one observes clear charge accumulation around the C atom and charge depletion on the neighboring Ni and surface atoms that participate in bonding. On the Ni supported models, the depletion lobes on Ni are particularly pronounced, and they extend toward the adsorbed carbon, confirming that electron density is drawn from the metal into the C centered states. This is exactly what would be expected for the formation of strong Ni C bonds, which are precursors to carbide like environments and finally to graphitic carbon structures under reaction conditions.

The agreement between EDD and Mulliken trends reinforces the conclusion that carbon behaves as a strong electronic sink at the metal support perimeter. From a mechanistic perspective, these results have several important implications. First, both alumina and Ni can bind atomic carbon very strongly, but Ni and especially the Ni alumina interface stabilize it more. This means that once C atoms are generated, for example by methane cracking on Ni or by CO dissociation, they will preferentially accumulate at or near Ni sites and interfaces, where

the binding is strongest. Second, hydroxylation of the support, which weakened CO_2 chemisorption, actually enhances C binding, particularly at the interface. This dual effect is subtle. On the one hand, stronger C binding can promote coke nucleation and make carbon more difficult to remove. On the other hand, hydroxyls and the associated changes in electronic structure may also facilitate oxidation pathways if CO_2 or H_2O are present, by stabilizing transition states and intermediates for C oxidation. The present adsorption results alone cannot distinguish these two possibilities; they clearly show that the thermodynamic driving force for C accumulation is high, but they do not directly address the barriers for C removal.

Finally, it is important to recognize the limitations of the present model. The calculations consider isolated C atoms at zero Kelvin and very low coverage. In real DRM conditions, carbon forms clusters, chains, graphene like layers and filamentous structures, whose energetics differ from those of isolated atoms. Entropic contributions and coadsorption of O, OH, CO and other species will also modify the effective stability and mobility of carbon. Nevertheless, the qualitative message is robust: Ni and the Ni alumina interface are intrinsically strong traps for carbon, and hydroxylation can further enhance this trapping at specific sites. Any realistic mitigation strategy must therefore focus not only on reducing the rate of carbon formation, for example by tuning CH_4 and CO_2 activation pathways, but also on promoting efficient oxidation and removal of strongly bound C species at the metal support perimeter.

Comparison of the species' adsorption energy with each other and with the literature

A comparative analysis of the adsorption energies obtained in this work and those reported in previous DFT studies on Ni based catalysts is summarized in Table 6. For CH_4, all systems show relatively small interaction energies, typically between about − 0.02 eV and − 0.66 eV.

In this work, CH_4 adsorption energies range from − 0.24 eV on α Al_2O_3(0001) to −0.38 eV on Ni/α Al_2O_3(0001), which places our values in the same order of magnitude as those reported for Ni(111), Ni/CaO, Ni/α MoC(111), Ni/MgO(100) and PtNi[79–84]. These consistently weak and only mildly system dependent values confirm that CH_4 is predominantly physisorbed on Ni based catalysts, without formation of strong chemical bonds to either the metal or the support. In other words, the rate controlling step in DRM is not the creation of a deep molecular adsorption well for CH_4, but the activation of the first C-H bond in the transition state, in line with the mechanistic picture developed in the previous sections.

In contrast, CO_2 shows much stronger and more system sensitive interactions. On bare α Al_2O_3(0001), CO_2 adsorption is already strongly exothermic, with an energy of −2.08 eV, reflecting the formation of a chemisorbed, bent carbonate like species. On α Al_2O_3 OH(0001) the interaction is much weaker, −0.53 eV, consistent with a physisorbed, nearly linear CO_2 state. The introduction of Ni at the metal support interface dramatically enhances CO_2 binding on both supports. The adsorption energy becomes − 2.33 eV on Ni/α Al_2O_3(0001) and − 2.43 eV on Ni/α Al_2O_3 OH(0001), accompanied by strong bending and significant charge transfer to CO_2. This shows that the Ni alumina interface reinstates and even surpasses the strong activation observed on pure α Al_2O_3(0001), even when the support is hydroxylated. Compared to the literature, our CO_2 adsorption on Ni/Al_2O_3 is more exothermic than on Ni/ZrO_2 (−1.29 eV), Ni/α MoC(111) (−0.91 eV) and Ni/CaO (−1.81 eV)[80–82]. This indicates that alumina, in combination with Ni, is particularly effective in stabilizing activated CO_2 species. The PDOS and charge analyses discussed earlier suggest that this is due to a favorable Al donor - Ni - CO_2 acceptor synergy that promotes charge redistribution at the interface.

CO adsorption further highlights the strong role of Ni. In our models, CO binds moderately on α Al_2O_3(0001) and α Al_2O_3 OH(0001) (about − 0.68 and − 0.71 eV), but much more strongly on Ni supported alumina, with adsorption energies of −1.66 eV and − 1.96 eV on Ni/α Al_2O_3(0001) and Ni/α Al_2O_3 OH(0001), respectively. Literature values for Ni(111), Ni/α MoC(111), Ni/MgO(100) and PtNi span a similar or slightly stronger range, from about − 1.92 eV to −3.49 eV[79,81,83,85]. These data confirm that CO is strongly bound to Ni sites, and that support effects can tune but not suppress this strong interaction. From a DRM perspective, this means that CO desorption and CO mediated oxidation steps must be considered carefully in any microkinetic model, especially given the well known competition between CO and CO_2 for adsorption sites on Ni.

	CH_4	CO_2	CO	H_2	C	Ni_2	Ref.
	This work						
Ni_2	−0.31	−1.12	−1.47	−0.78	−4.33	-	-
Pure Al_2O_3	−0.24	−2.08	−0.68	−0.20	−3.54	-	-
OH-Al_2O_3	−0.31	−0.53	−0.71	−0.21	−4.41	-	-
Ni/Pure Al_2O_3	−0.38	−2.33	−1.66	−0.12	−6.22	−1.60	-
Ni/OH- Al_2O_3	−0.33	−2.43	−1.96	+0.32	−6.47	−1.85	-
	Literature						
Ni (111)	−0.02	−0.02	−1.92	−0.22	−6.78	-	79
Ni/ZrO_2	−0.66	−1.29	−3.49	-	−9.21	-	80
Ni/αMoC (111)	−0.39	−0.91	−1.92	−0.48	−6.77	-	81
Ni/CaO	−0.18	−1.81	−0.46	−0.16	-	-	82
Ni/MgO (100)	−0.02	−0.03	−2.42	−0.44	−8.14	-	83
PtNi	−0.28	−0.60	−2.53	−1.19	−7.10	-	84

Table 6. Adsorption energies (eV) of the CH_4, CO_2, CO, H_2, C, and Ni_2 species over the modeled catalysts.

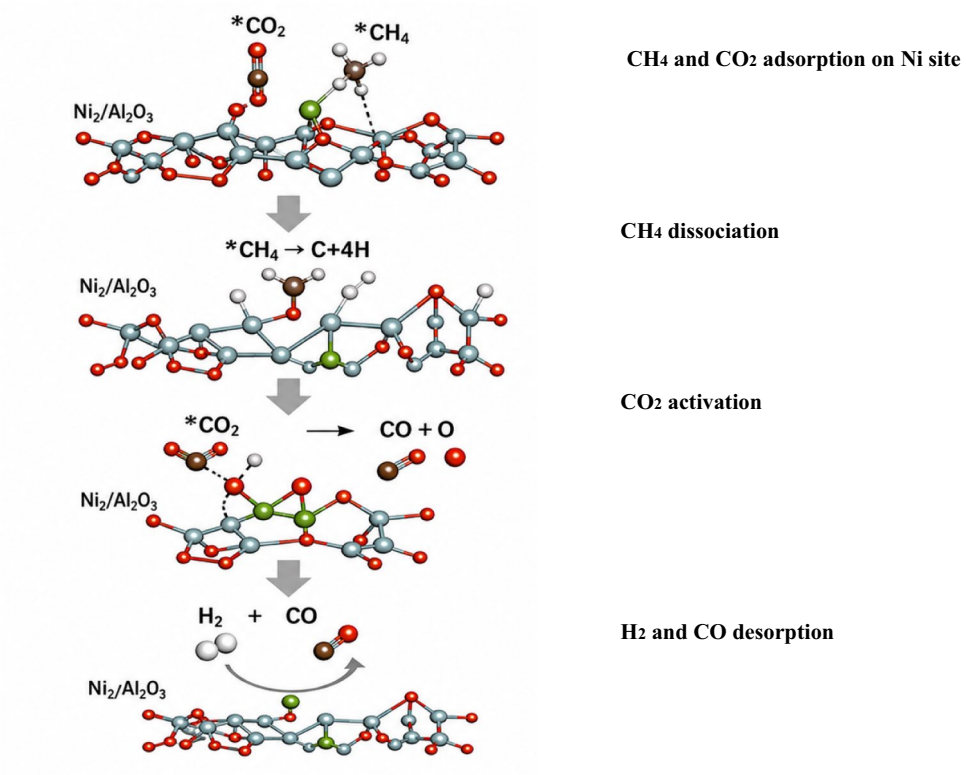


Fig. 16. Reaction pathway and coordination figure.

For H_2, our results are again consistent with the view that molecular hydrogen is only weakly bound on Ni based catalysts. In this work, H_2 adsorption energies are modestly exothermic on α Al_2O_3(0001) and α Al_2O_3 OH(0001) (−0.20 and − 0.21 eV), even weaker on Ni/α Al_2O_3(0001) (−0.12 eV), and endothermic on Ni/α Al_2O_3 OH(0001) (0.32 eV), indicating no stable molecular adsorption well on the latter. Literature values on Ni(111), Ni/α MoC(111) and Ni/MgO(100) are also small in magnitude (−0.22 to −0.48 eV)[79,81,85]. Only PtNi stands out with a significantly stronger H_2 interaction (−1.19 eV)[85]. Overall, this comparison supports the conclusion that H_2 remains largely physisorbed on Ni alumina catalysts. This weak interaction is beneficial, since it facilitates H_2 desorption and prevents blocking of active sites by molecular hydrogen, in agreement with the mechanistic picture where Ni is crucial for stabilizing surface H atoms and lowering H-H recombination barriers, rather than for strongly binding H_2.

The situation is very different for atomic carbon. In this work, C adsorption energies are already large on pure α Al_2O_3(0001) and α Al_2O_3 OH(0001) (−3.54 and − 4.41 eV), and become even more exothermic on Ni supported systems, −6.22 eV on Ni/α Al_2O_3(0001) and − 6.47 eV on Ni/α Al_2O_3 OH(0001). Literature values for Ni(111), Ni/ZrO_2, Ni/α MoC(111), Ni/MgO(100) and PtNi range from about − 6.77 to −9.21 eV[79–81,83,85], indicating that some supports, such as ZrO_2 or MgO, can stabilize C even more strongly than alumina. Thus, Ni supported alumina is not the worst case in terms of carbon trapping, but it still provides a very strong thermodynamic driving force for C accumulation. Combined with the kinetic ease of CH_4 cracking on Ni, this explains the high propensity of Ni based DRM catalysts to coke. The strong stabilization of C at the Ni alumina interface, especially in the presence of hydroxyl groups, matches the picture that hydroxylated surfaces can both promote stronger adsorbate binding and complicate carbon removal, unless CO_2 or H_2O oxidation pathways are efficient.

Finally, the Ni dimer adsorption energetics themselves are consistent with a strong metal support interaction. The adsorption energies of Ni_2 on α Al_2O_3(0001) and α Al_2O_3 OH(0001) are − 1.60 eV and − 1.85 eV, respectively. The more negative value on the hydroxylated surface implies a stronger anchoring of Ni species, which can improve dispersion and thermal stability, but at the price of further enhancing the interaction with strongly binding adsorbates such as C. This dual effect of hydroxyls, simultaneously stabilizing Ni and increasing the binding strength of key intermediates, is a recurring theme in our results.

These energetic trends can be summarized in the schematic reaction pathway for DRM over Ni_2/Al_2O_3 shown in Fig. 16. The catalytic cycle begins with co adsorption of CH_4 and CO_2 on the Ni supported alumina surface. Methane is weakly physisorbed, then undergoes stepwise dissociative adsorption on Ni sites to produce surface carbon (*C) and hydrogen atoms (*H). CO_2, which is strongly activated at the Ni alumina interface, is reduced to CO while generating surface oxygen species (*O). Subsequent elementary steps involve recombination and desorption of H_2 and CO, and the oxidation of *C by *O or CO_2 derived intermediates.

The relative adsorption energies of CH_4, CO_2, CO, H_2 and C on the different sites rationalize the overall picture. Ni sites are crucial for C-H and C = O bond activation and for stabilizing reactive intermediates, alumina

and its hydroxylation state tune charge transfer and the strength of adsorbate binding, and the metal support interface emerges as the key region controlling both activity and coking tendency in DRM on Ni based catalysts.

Conclusion

This work provides an atomistic description of key elementary steps in dry reforming of methane on Ni supported alumina, using DFT + U+D2 calculations for CH_4, CO_2, H_2, atomic C and Ni_2 on α Al_2O_3(0001), α Al_2O_3 OH(0001) and their Ni supported counterparts. Validation against experimental and theoretical reference data for small molecules, Ni_2 and bulk α Al_2O_3 shows that the chosen computational setup reliably captures both molecular and metallic bonding, including the subtle effect of surface hydroxylation on alumina.

Across all systems, CH_4 adsorption is weak and only mildly dependent on the presence of Ni or surface hydroxyls, and the molecule remains essentially tetrahedral. Together with literature data, this confirms that intact methane interacts mainly via physisorption and is not significantly preactivated in the initial state. H_2 shows similarly weak or even unstable molecular adsorption on all models, with negligible structural or electronic changes. These findings indicate that the catalytic role of Ni in DRM does not arise from strong molecular binding of CH_4 or H_2, but from its ability to lower the barriers for C H bond cleavage and for recombination of surface H atoms into H_2.

In contrast, CO_2 exhibits a rich and highly support dependent behaviour. On α Al_2O_3(0001) it forms strongly chemisorbed, bent carbonate like species with large adsorption energies, whereas hydroxylation of the surface suppresses this activation and leads to a nearly linear, weakly bound CO_2. When Ni is introduced, the Ni/α Al_2O_3(0001) and Ni/α Al_2O_3 OH(0001) interfaces restore and even enhance CO_2 activation. Very exothermic adsorption energies, pronounced O C O bending and strong electronic hybridisation between Ni, Al and CO_2 states reveal a cooperative Al donor, Ni, CO_2 acceptor motif located at the metal support perimeter. The Mulliken charge and electron density difference analyses show that this interface acts as a powerful charge donor to CO_2, which rationalises its superior activation compared with other Ni based systems reported in the literature.

CO behaves as a sensitive probe of the same interfacial chemistry. It is only weakly physisorbed on bare alumina, but becomes strongly chemisorbed on Ni supported alumina, especially at the hydroxylated perimeter where the C O bond is almost completely broken and the adsorbate is electronically coupled to a multi centre Ni Ni Al environment. Atomic carbon is even more strongly stabilised, with adsorption energies that are substantially more exothermic on Ni containing models than on bare alumina and are further enhanced by hydroxylation. Projected density of states, Mulliken charges and electron density difference maps consistently show intense Ni C hybridisation and significant charge transfer from the Ni dimer and the Al O framework to the adsorbed C atom. These features identify the Ni alumina interface, and particularly its hydroxylated form, as an intrinsic trap for carbon and therefore as a critical locus for coke nucleation.

Comparison with other Ni based catalysts from the literature confirms that Ni supported alumina is especially effective for CO_2 activation, but still provides a strong thermodynamic driving force for carbon accumulation. The overall picture that emerges is that Ni sites are responsible for CH_4 dehydrogenation and H recombination, the Ni alumina perimeter is the main region for CO_2 activation and C oxidation, and the alumina support, including its hydroxylation state, tunes charge transfer and the binding strength of reactive intermediates. The microscopic descriptors extracted here, in particular the relative adsorption energies of CH_4, CO_2, CO, H_2 and C, the identified Al donor, Ni, adsorbate acceptor pattern and the electronic fingerprints of interfacial Ni C and Ni CO_2 bonding, provide concrete targets for rational catalyst design. Strategies such as controlled surface hydroxylation, modification of the alumina support or alloying of Ni to weaken Ni C interactions while preserving efficient CO_2 activation at the metal support interface appear especially promising for developing Ni based DRM catalysts that combine high activity with improved resistance to coking.

Data availability

All the data generated was present in the submitted manuscript.

Received: 3 January 2026; Accepted: 9 July 2026
Published online: 27 July 2026

References

1. Cutad, M. B., Al-Marri, M. J. & Kumar, A. Recent developments on CO2 hydrogenation performance over structured zeolites: A review on properties, synthesis, and characterization. *Catalysts* **14**, 328. https://doi.org/10.3390/catal14050328 (2024).
2. Cui, L. et al. A review of catalytic hydrogenation of carbon dioxide: From waste to hydrocarbons. *Front. Chem.* **10**, 1037997. https://doi.org/10.3389/fchem.2022.1037997 (2022).
3. Omar Noraziah, Z. M., Afiq, R. W. M. F., Wan, H., Haslenda, N. J. & Le Ho Wai Shin. Study of Carbon Dioxide Methanation Performance using Nickel-Based Catalyst and New Synthesised Catalyst. *Chem. Eng. Trans.* **106**, 805–810. https://doi.org/10.3303/CET23106135 (2023).
4. Yamaoka, M., Tomozawa, K., Sumiyoshi, K., Ueda, T. & Ogo, S. Efficient reverse water gas shift reaction at low temperatures over an iron supported catalyst under an electric field. *Sci. Rep.* **14**, 10216. https://doi.org/10.1038/s41598-024-61017-2 (2024).
5. Wang, H. et al. Facilitating the dry reforming of methane with interfacial synergistic catalysis in an Ir@CeO2−x catalyst. *Nat. Commun.* **15**, 3765. https://doi.org/10.1038/s41467-024-48122-6 (2024).
6. Legutko, P. et al. Functional improvement of NiOx/CeO2 model catalyst active in dry methane reforming via optimization of nickel content. *Processes* **12**, 851. https://doi.org/10.3390/pr12050851 (2024).
7. Legutko, P., Kozieł, M., Kowalczyk, A., Michalik, M. & Adamski, A. Effect of active phase precursor on structural, textural and catalytic properties of the model NiOx/CeO2 system active in dry reforming of methane. *Crystals* **14**, 634. https://doi.org/10.3390/cryst14070634 (2024).
8. Abdulrasheed, A. et al. A review on catalyst development for dry reforming of methane to syngas: Recent advances. *Renew. Sustain. Energy Rev.* **108**, 175–193. https://doi.org/10.1016/j.rser.2019.03.054 (2019).

9. Yoo, E. et al. Effects of operating parameters and feed gas compositions on the dry reforming of methane over the Ni/Al2O3 catalyst. *Catalysts* **13**, 602. https://doi.org/10.3390/catal13030602 (2023).
10. Dehimi, L., Gaillard, M., Virginie, M., Erto, A. & Benguerba, Y. Investigation of dry reforming of methane over Mo-based catalysts. *Int. J. Hydrog. Energy*. **45**, 24657–24669. https://doi.org/10.1016/j.ijhydene.2020.06.203 (2020).
11. Bakar, S. N. S. S. A. et al. Catalytic performance of bimetallic cobalt–nickel/graphene oxide for carbon dioxide reforming of methane. *ChemEngineering* **7**, 107. https://doi.org/10.3390/chemengineering7060107 (2023).
12. Jang, W-J., Shim, J-O., Kim, H-M., Yoo, S-Y. & Roh, H-S. A review on dry reforming of methane in aspect of catalytic properties. *Catal. Today*. **324**, 15–26. https://doi.org/10.1016/j.cattod.2018.07.032 (2019).
13. Singh, S. et al. Boron-doped Ni/SBA-15 catalysts with enhanced coke resistance and catalytic performance for dry reforming of methane. *J. Energy Inst.* **93**, 31–42. https://doi.org/10.1016/j.joei.2019.04.011 (2020).
14. Chein, R-Y. & Fung, W-Y. Syngas production via dry reforming of methane over CeO2 modified Ni/Al2O3 catalysts. *Int. J. Hydrog. Energy*. **44**, 14303–14315. https://doi.org/10.1016/j.ijhydene.2019.01.113 (2019).
15. Sasson Bitters, J. et al. Utilizing bimetallic catalysts to mitigate coke formation in dry reforming of methane. *J. Energy Chem.* **68**, 124–142. https://doi.org/10.1016/j.jechem.2021.11.041 (2022).
16. Niu, J., Liland, S. E., Yang, J., Rout, K. R., Ran, J., & Chen, D.. Effect of oxide additives on the hydrotalcite derived Ni catalysts for CO_2 reforming of methane. *Chem. Eng. J.*, **377**, 119763. https://doi.org/10.1016/j.cej.2018.08.149 (2019).
17. IEA, Global Methane Tracker Paris, I. E. A. (2023). https://www.iea.org/reports/global-methane-tracker-2023, Licence: CC BY 4.0 2023.
18. Schwengber, C. A. et al. Methane dry reforming using Ni/Al2O3 catalysts: Evaluation of the effects of temperature, space velocity and reaction time. *J. Environ. Chem. Eng.* **4**, 3688–3695. https://doi.org/10.1016/j.jece.2016.07.001 (2016).
19. Xiao, H. et al. Highly efficient Ni/Ac-Al2O3 catalysts in the dry reforming of methane: influence of acetic acid treatment and Ni loading. *RSC Adv.* **14**, 39061–39068. https://doi.org/10.1039/D4RA06740A (2024).
20. Xu, Z. & Park, E. D. Recent Advances in Coke Management for Dry Reforming of Methane over Ni-Based Catalysts. *Catalysts* **14**, 176. https://doi.org/10.3390/catal14030176 (2024).
21. Wysocka, I., Hupka, J. & Rogala, A. Catalytic activity of nickel and ruthenium–nickel catalysts supported on SiO2, ZrO2, Al2O3, and MgAl2O4 in a dry reforming process. *Catalysts* **9**, 540. https://doi.org/10.3390/catal9060540 (2019).
22. Alioui, O. et al. Contribution of DFT to the optimization of Ni-based catalysts for dry reforming of methane: a review. *Catal. Reviews*. **65**, 1468–1520. https://doi.org/10.1080/01614940.2021.2020518 (2023).
23. Dekkar, S. et al. Dry Reforming of Methane over Ni–Al2O3 and Ni–SiO2 Catalysts: Role of Preparation Methods. *Catal. Lett.* **150**, 2180–2199. https://doi.org/10.1007/s10562-020-03120-3 (2020).
24. Pérez-Madrigal, V., Ríos-Valdovinos, E., Rojas-García, E., Valenzuela, M. A. & Pola-Albores, F. Dry Reforming of Methane over Li-Doped Ni/TiO2 Catalysts: Effect of Support Basicity. *Methane* **2**, 452–469. https://doi.org/10.3390/methane2040031 (2023).
25. Fakeeha, A. H. et al. Fe-promoted alumina-supported Ni catalyst stabilized by zirconia for methane dry reforming. *Catalysts* **13**, 806. https://doi.org/10.3390/catal13050806 (2023).
26. Manabayeva, A. M. et al. Dry reforming of methane over Mn-modified Ni-based catalysts. *Catal. Lett.* **154**, 4780–94. https://doi.org/10.1007/s10562-024-04676-0 (2024).
27. Araiza, D. G., Arcos, D. G., Gómez-Cortés, A. & Díaz, G. Dry reforming of methane over Pt-Ni/CeO2 catalysts: Effect of the metal composition on the stability. *Catal. Today* **360**, 46–54. https://doi.org/10.1016/j.cattod.2019.06.018 (2021).
28. Alipour, Z., Rezaei, M. & Meshkani, F. Effect of alkaline earth promoters (MgO, CaO, and BaO) on the activity and coke formation of Ni catalysts supported on nanocrystalline Al2O3 in dry reforming of methane. *J. Ind. Eng. Chem.* **20**, 2858–2863. https://doi.org/10.1016/j.jiec.2013.11.018 (2014).
29. Tyo, E. C. & Vajda, S. Catalysis by clusters with precise numbers of atoms. *Nat. Nanotech.* **10**, 577–588. https://doi.org/10.1038/nnano.2015.140 (2015).
30. Wang, W. et al. Mixed-Phase Oxide Catalyst Based on Mn-Mullite (Sm, Gd)Mn_2O_5 for NO Oxidation in Diesel Exhaust. *Science* **337**, 832–835. https://doi.org/10.1126/science.1225091 (2012).
31. Dong, S., Zhang, Y., Zhang, X., Mao, J. & Yang, Z. A possible highly active supported Ni dimer catalyst for O2 dissociation: A first-principles study. *Appl. Surf. Sci.* **402**, 168–74. https://doi.org/10.1016/j.apsusc.2017.01.057 (2017).
32. Chen, J., Sharapa, D. & Plessow, P. N. Stability and formation of hydroxylated α – Al_2O_3 (0001) surfaces at high temperatures. *Phys. Rev. Res.* **4**, 013232. https://doi.org/10.1103/PhysRevResearch.4.013232 (2022).
33. Akça, A. CH4 dissociation on the Pd/Cu(111) surface alloy: A DFT study. *Open. Phys.* **18**, 790–798. https://doi.org/10.1515/phys-2020-0195 (2020).
34. Niu, J. et al. Impact of Ni particle size on CO2 activation and CO formation during reforming process: A density functional theory study. *Front. Energy*. **18**, 525–534. https://doi.org/10.1007/s11708-024-0952-6 (2024).
35. Zhang, C. et al. Effect of Cu doping on Ni surface on CO formation pathways during the methane dry reforming reaction. *Mol. Catal.* **560**, 114125. https://doi.org/10.1016/j.mcat.2024.114125 (2024).
36. Lagauche, M. et al. Thermodynamic Characterization of the Hydroxyl Group on the γ-Alumina Surface by the Energy Distribution Function. *J. Phys. Chem. C.* **121**, 16770–16782. https://doi.org/10.1021/acs.jpcc.7b02498 (2017).
37. Peng, H. & Perdew, J. P. Rehabilitation of the Perdew-Burke-Ernzerhof generalized gradient approximation for layered materials. *Phys. Rev. B* **95**, 081105. https://doi.org/10.1103/PhysRevB.95.081105 (2017).
38. He, L. et al. Accuracy of generalized gradient approximation functionals for density-functional perturbation theory calculations. *Phys. Rev. B* **89**, 064305. https://doi.org/10.1103/PhysRevB.89.064305 (2014).
39. Zhang, L. et al. Theoretical study on dry reforming of methane catalyzed by Cu12M (M = Cu, Fe, Co, Ni) core-shell bimetallic clusters. *Fuel* **303**, 121263. https://doi.org/10.1016/j.fuel.2021.121263 (2021).
40. Newnham, R. E. & De Haan, Y. M. Refinement of the α Al2O3, Ti2O3, V2O3 and Cr2O3 structures. *Z. Kristallogr.* **117**, 235–7. https://doi.org/10.1524/zkri.1962.117.2-3.235 (1962).
41. Wang, X. G., Chaka, A., & Scheffler, M.. Effect of the environment on alpha-Al2O3 (0001) surface structures. *Phys. Rev. lett.*, **84** (16), 3650–3653. https://doi.org/10.1103/PhysRevLett.84.3650 (2000).
42. Zhang, G. et al. First principles investigation of helium physisorption on an α-Al2O3 (0001) surface. *Phys. Chem. Chem. Phys.* **18**, 15711–15718. https://doi.org/10.1039/C6CP01517D (2016).
43. Jiang, M., Nie, B., Yang, Z., Ni, M. & Chen, Z. First principles investigation of hydrogen adsorption and dissociation on Fe doped α-Al2O3 (0001) surface. *J. Nucl. Mater.* **533**, 152102. https://doi.org/10.1016/j.jnucmat.2020.152102 (2020).
44. Sholl, D. S. & Steckel, J. A. *Density Functional Theory: A Practical Introduction* 1st ed. (Wiley, 2009). https://doi.org/10.1002/9780470447710.
45. Piontek, S. M. et al. Probing Heterogeneous Charge Distributions at the α-Al_2O_3 (0001)/H_2O Interface. *J. Am. Chem. Soc.* **142**, 12096–12105. https://doi.org/10.1021/jacs.0c01366 (2020).
46. DelloStritto, M. J., Piontek, S. M., Klein, M. L. & Borguet, E. Effect of functional and electron correlation on the structure and spectroscopy of the Al_2O_3 (001)–H_2O interface. *J. Phys. Chem. Lett.* **10**, 2031–6. https://doi.org/10.1021/acs.jpclett.9b00016 (2019).
47. Yang, D., Krasowska, M., Sedev, R. & Ralston, J. The unusual surface chemistry of α-Al2O3 (0001). *Phys. Chem. Chem. Phys.* **12**, 13724. https://doi.org/10.1039/c001222j (2010).
48. Fu, Q., Wagner, T. & Rühle, M. Hydroxylated α-Al2O3 (0001) surfaces and metal/α-Al2O3 (0001) interfaces. *Surf. Sci.* **600**, 4870–4877. https://doi.org/10.1016/j.susc.2006.08.008 (2006).

49. Altarawneh, M., Assaf, N. W., Hussain, H. M. & Dlugogorski, B. Z. Structural properties of alumina surfaces and their roles in the synthesis of environmentally persistent free radicals (EPFRs). *Nanotechnology Reviews* **12**, 20220536. https://doi.org/10.1515/ntrev-2022-0536 (2023).
50. McHale, J. M., Auroux, A., Perrotta, A. J. & Navrotsky, A. Surface energies and thermodynamic phase stability in nanocrystalline aluminas. *Science* **277**, 788–91. https://doi.org/10.1126/science.277.5327.788 (1997).
51. Stanton, J. F. A refined estimate of the bond length of methane. *Mol. Phys.* **97**, 841–5. https://doi.org/10.1080/00268979909482885 (1999).
52. Truong, T. N., Truhlar, D. G., Baldridge, K. K., Gordon, M. S. & Steckler, R. Transition state structure, barrier height, and vibrational frequencies for the reaction Cl+CH_4→CH_3 + HCl. *J. Chem. Phys.* **90**, 7137–42. https://doi.org/10.1063/1.456244 (1989).
53. Klotz, A., Ward, T. & Dartois, E. Molecular complexes theoretical computations between methanol and carbon dioxide and their implications in the interstellar ice mantles. *A&A* **416**, 801–10. https://doi.org/10.1051/0004-6361:20034602 (2004).
54. Glockler, G. Carbon–Oxygen Bond Energies and Bond Distances. *J. Phys. Chem.* **62**, 1049–1054. https://doi.org/10.1021/j150567a006 (1958).
55. Broqvist, P. A DFT Study on CO Oxidation over Co3O4. *J. Catal.* **210**, 198–206. https://doi.org/10.1006/jcat.2002.3678 (2002).
56. Wu, T. et al. Efficient reclamation of carbon fibers from epoxy composite waste through catalytic pyrolysis in molten $ZnCl_2$. *RSC Adv.* **9**, 377–388. https://doi.org/10.1039/C8RA08958B (2019).
57. Song, Z. et al. Adsorption properties of CO, H2 and CH4 over Pd/γ-Al2O3 catalyst: A density functional study. *Appl. Surf. Sci.* **387**, 341–350. https://doi.org/10.1016/j.apsusc.2016.06.077 (2016).
58. Hensel, F. & Edwards, P. P. Hydrogen, the First Alkali Metal. *Chem. Eur. J.* **2**, 1201–1203. https://doi.org/10.1002/chem.19960021005 (1996).
59. Goodwin, L., Skinner, A. J. & Pettifor, D. G. Generating Transferable Tight-Binding Parameters: Application to Silicon. *Europhys. Lett.* **9**, 701–706. https://doi.org/10.1209/0295-5075/9/7/015 (1989).
60. Liu, Z., Wang, Y., Li, J. & Zhang, R. The effect of γ-Al2O3 surface hydroxylation on the stability and nucleation of Ni in Ni/γ-Al2O3 catalyst: a theoretical study. *RSC Adv.* **4**, 13280. https://doi.org/10.1039/c3ra46352d (2014).
61. Toofan, J. & Watson, P. R. The termination of the a-Al2 O3 (0001) surface: a LEED crystallography determination. *Surf. Sci.* **401**, 162–172. https://doi.org/10.1016/S0039-6028(97)01031-5 (1998).
62. Briquet, L. G. V., Catlow, C. R. A. & French, S. A. Comparison of the adsorption of Ni, Pd, and Pt on the (0001) surface of α-alumina. *J. Phys. Chem. C* **112**, 18948–54. https://doi.org/10.1021/jp803540r (2008).
63. Niu, J. et al. New mechanism insights into methane steam reforming on Pt/Ni from DFT and experimental kinetic study. *Fuel* **266**, 117143. https://doi.org/10.1016/j.fuel.2020.117143 (2020).
64. Gao, Y., Hou, G., Cao, J., Zhang, S. & Li, Z. Molecular simulation of CH4 adsorption characteristics under the coupling of different temperature and water content. *Appl. Sci.* **14**, 8757. https://doi.org/10.3390/app14198757 (2024).
65. Zhang, M., Yu, Y. & Zhang, Y. DFT research of methane preliminary dissociation on aluminum catalyst. *Appl. Surf. Sci.* **280**, 15–24. https://doi.org/10.1016/j.apsusc.2013.04.058 (2013).
66. Zhang, M., Yang, K., Zhang, X. & Yu, Y. Effect of Ni(111) surface alloying by Pt on partial oxidation of methane to syngas: A DFT study. *Surf. Sci.* **630**, 236–243. https://doi.org/10.1016/j.susc.2014.08.023 (2014).
67. Díaz López, E. & Comas-Vives, A. CO2 activation dominating the dry reforming of methane catalyzed by Rh(111) based on multiscale modelling. *Catal. Sci. Technol.* **13**, 7162–71. https://doi.org/10.1039/D3CY01546G (2023).
68. Guharoy, U., Le Saché, E., Cai, Q., Reina, T. R. & Gu, S. Understanding the role of Ni-Sn interaction to design highly effective CO2 conversion catalysts for dry reforming of methane. *J. CO2 Util.* **27**, 1–10. https://doi.org/10.1016/j.jcou.2018.06.024 (2018).
69. Casarin, M., Falcomer, D., Glisenti, A. & Vittadini, A. Experimental and theoretical study of the interaction of CO2 with α-Al2O3. *Inorg. Chem.* **42**, 436–45. https://doi.org/10.1021/ic0257773 (2003).
70. Rohmann, C., Metson, J. B. & Idriss, H. DFT study of carbon monoxide adsorption on α-Al_2O_3(0001). *Surf. Sci.* **605**, 1694–703. https://doi.org/10.1016/j.susc.2011.05.033 (2011).
71. Dehimi, L., Benguerba, Y., Virginie, M. & Hijazi, H. Microkinetic modelling of methane dry reforming over Ni/Al_2O_3 catalyst. *Int. J. Hydrogen Energy* **42**, 18930–40. https://doi.org/10.1016/j.ijhydene.2017.05.231 (2017).
72. Zhang, M., Chen, J., Yu, Y. & Zhang, Y. DFT study on the structure of Ni/α-Al2O3 catalysts. *Appl. Surf. Sci.* **287**, 97–107. https://doi.org/10.1016/j.apsusc.2013.09.082 (2013).
73. Manabayeva, A. M. et al. Dry Reforming of Methane over Ni–Fe–Al Catalysts Prepared by Solution Combustion Synthesis. *Ind. Eng. Chem. Res.* **62**, 11439–11455. https://doi.org/10.1021/acs.iecr.3c00272 (2023).
74. Akri, M. et al. Atomically dispersed nickel as coke-resistant active sites for methane dry reforming. *Nat. Commun.* **10**, 5181. https://doi.org/10.1038/s41467-019-12843-w (2019).
75. Benguerba, Y., Dehimi, L., Virginie, M., Dumas, C. & Ernst, B. Modelling of methane dry reforming over Ni/Al2O3 catalyst in a fixed-bed catalytic reactor. *React. Kinet. Mech. Catal.* **114**, 109–19. https://doi.org/10.1007/s11144-014-0772-5 (2015).
76. Benguerba, Y., Dehimi, L., Virginie, M., Dumas, C. & Ernst, B. Numerical investigation of the optimal operative conditions for the dry reforming reaction in a fixed-bed reactor: Role of the carbon deposition and gasification reactions. *React. Kinet. Mech. Catal.* **115**, 483–97. https://doi.org/10.1007/s11144-015-0849-9 (2015).
77. Chen, S., Zaffran, J. & Yang, B. Dry reforming of methane over the cobalt catalyst: Theoretical insights into the reaction kinetics and mechanism for catalyst deactivation. *Appl. Catal. B Environ.* **270**, 118859. https://doi.org/10.1016/j.apcatb.2020.118859 (2020).
78. Abdulrasheed, A. et al. A review on catalyst development for dry reforming of methane to syngas: Recent advances. *Renew. Sustain. Energy Rev.* **108**, 175–193. https://doi.org/10.1016/j.rser.2019.03.054 (2019).
79. Zhu, Y.-A., Chen, D., Zhou, X.-G. & Yuan, W.-K. DFT studies of dry reforming of methane on Ni catalyst. *Catal. Today* **148**, 260–7. https://doi.org/10.1016/j.cattod.2009.08.022 (2009).
80. Dou, J. et al. Sandwiched SiO2@Ni@ZrO2 as a coke resistant nanocatalyst for dry reforming of methane. *Appl. Catal. B.* **254**, 612–623. https://doi.org/10.1016/j.apcatb.2019.05.021 (2019).
81. Zou, X. et al. Density functional theory and kinetic Monte Carlo simulation study the strong metal–support interaction of dry reforming of methane reaction over Ni based catalysts. *Chin. J. Chem. Eng.* **29**, 176–82. https://doi.org/10.1016/j.cjche.2020.05.009 (2021).
82. Zhao, B. et al. Adsorption characteristics of gas molecules (H_2O, CO_2, CO, CH_4, and H_2) on CaO-based catalysts during biomass thermal conversion with in situ CO_2 capture. *Catalysts* **9**, 757. https://doi.org/10.3390/catal9090757 (2019).
83. Guo, Y., Feng, J. & Li, W. Effect of the Ni size on CH4/CO2 reforming over Ni/MgO catalyst: A DFT study. *Chin. J. Chem. Eng.* **25**, 1442–1448. https://doi.org/10.1016/j.cjche.2017.03.024 (2017).
84. Zhang, L., Meng, Y., Xie, B. & Xia, S. Theoretical investigation onto the reaction mechanism of dry reforming of methane on core–shell Cu-Ni-Pt ternary alloy clusters. *Chem. Phys. Lett.* **781**, 138975. https://doi.org/10.1016/j.cplett.2021.138975 (2021).
85. Zhang, L. et al. Theoretical study on dry reforming of methane catalyzed by Cu12M (M = Cu, Fe, Co, Ni) core-shell bimetallic clusters. *Fuel* **303**, 121263. https://doi.org/10.1016/j.fuel.2021.121263 (2021).

Acknowledgements

This study has been supported by the Midcareer Research Program (Grant No. RS-2025-00520940) of the Ministry of Education and the Government of the Republic of Korea. This research was also supported by the "Regional Innovation System & Education (RISE)" through the Seoul RISE Center, funded by the Ministry of Education

(MOE) and the Seoul Metropolitan Government. (2026-RISE-01-027-01).

Author contributions

S.S. performed the DFT calculations, built the slab and Ni_2 models, carried out adsorption and electronic structure analyses, and prepared the original draft. O.A. contributed to model validation, adsorption energy analysis, and interpretation of surface–adsorbate interactions. L.D. contributed to conceptualization of the study and critical interpretation of catalytic mechanisms. M.B. and A.E. provided methodological guidance on computational catalysis and contributed to data interpretation. M.A., M.A., and K.S.A.H. contributed to literature analysis and discussion of catalytic relevance. B.-H.J. and H.-J.A. supervised the work and contributed to funding acquisition and critical manuscript revision. Y.B. conceived the study, supervised the computational strategy, validated the results, and led manuscript review and editing. All authors reviewed and approved the final manuscript.

Funding

This study has been supported by the Midcareer Research Program (Grant No. RS-2025-00520940k) of the Ministry of Education and the Government of the Republic of Korea. This research was also supported by the "Regional Innovation System & Education (RISE)" through the Seoul RISE Center, funded by the Ministry of Education (MOE) and the Seoul Metropolitan Government. (2026-RISE-01-027-01).

Declarations

Competing interests

The authors declare no competing interests.

Additional information

Supplementary Information The online version contains supplementary material available at https://doi.org/10.1038/s41598-026-62218-7.

Correspondence and requests for materials should be addressed to B.-H.J. or Y.B.

Reprints and permissions information is available at www.nature.com/reprints.

Publisher's note Springer Nature remains neutral with regard to jurisdictional claims in published maps and institutional affiliations.

Open Access This article is licensed under a Creative Commons Attribution-NonCommercial-NoDerivatives 4.0 International License, which permits any non-commercial use, sharing, distribution and reproduction in any medium or format, as long as you give appropriate credit to the original author(s) and the source, provide a link to the Creative Commons licence, and indicate if you modified the licensed material. You do not have permission under this licence to share adapted material derived from this article or parts of it. The images or other third party material in this article are included in the article's Creative Commons licence, unless indicated otherwise in a credit line to the material. If material is not included in the article's Creative Commons licence and your intended use is not permitted by statutory regulation or exceeds the permitted use, you will need to obtain permission directly from the copyright holder. To view a copy of this licence, visit http://creativecommons.org/licenses/by-nc-nd/4.0/.

© The Author(s) 2026